
Sparsity-Controllable Dynamic Top- p MoE for Large Foundation Model Pre-training

Can Jin^{1*} Hongwu Peng^{2*} Mingcan Xiang^{2,3} Qixin Zhang⁴
 Xiangchi Yuan⁵ Amit Hasan² Ohiremen Dibia² Yifan Gong²
 Yan Kang^{2†} Dimitris N. Metaxas^{1†}

¹Rutgers University ²Adobe Research ³UMass Amherst
⁴Nanyang Technological University ⁵Georgia Institute of Technology

Abstract

Sparse Mixture-of-Experts (MoE) architectures effectively scale model capacity by activating only a subset of experts for each input token. However, the standard Top- k routing strategy imposes a uniform sparsity pattern that ignores the varying difficulty of tokens. While Top- p routing offers a flexible alternative, existing implementations typically rely on a fixed global probability threshold, which results in uncontrolled computational costs and sensitivity to hyperparameter selection. In this paper, we propose DTop- p MoE, a sparsity-controllable dynamic Top- p routing mechanism. To resolve the challenge of optimizing a non-differentiable threshold, we utilize a Proportional-Integral (PI) controller that dynamically adjusts the probability threshold to align the running activated-expert sparsity with a specified target. Furthermore, we introduce a dynamic routing normalization mechanism that adapts layer-wise routing logits, allowing different layers to learn distinct expert-selection patterns while utilizing a global probability threshold. Extensive experiments on Large Language Models and Diffusion Transformers demonstrate that DTop- p consistently outperforms both Top- k and fixed-threshold Top- p baselines. Our analysis confirms that DTop- p maintains precise control over the number of activated experts while adaptively allocating resources across different tokens and layers. Furthermore, DTop- p exhibits strong scaling properties with respect to expert granularity, expert capacity, model size, and dataset size, offering a robust framework for large-scale MoE pre-training.

1 Introduction

The recent development of large foundation models (LFMs) [19, 32, 38, 39, 44] has been driven largely by the observation that scaling model capacity reliably improves performance across modalities and tasks [28]. However, simply increasing model size quickly encounters computational and memory constraints. Consequently, Sparse Mixture-of-Experts (MoE) architectures have become a primary component of state-of-the-art systems [14, 29, 48, 50, 53, 54]. By activating only a small subset of experts for each token, MoE models scale parameter count and training throughput simultaneously, often outperforming dense counterparts while remaining trainable in parallel [12, 37].

Most existing MoE systems rely on Top- k routing: for every token at every layer, the router selects exactly k experts [12, 14, 37, 53]. While computationally efficient and hardware-friendly, this design enforces a uniform sparsity pattern across tokens and layers. In practice, however, different tokens exhibit distinct routing requirements: complex or rare tokens may benefit from more experts, while

* Equal Contribution, † Equal Advising. Correspondence to: Can Jin <can.jin@rutgers.edu>. Work done during an internship at Adobe Research.

simple or redundant tokens may require fewer [23, 27]. To address this, recent works explore Top- p routing, which selects experts whose cumulative routing probabilities exceed a fixed threshold, thereby allowing different tokens to activate varying numbers of experts [23, 55]. Yet, current Top- p variants face two primary limitations: (i) they typically utilize a global, fixed probability threshold, which is unlikely to remain optimal throughout the entire training process; and (ii) the number of activated experts is uncontrolled, which presents significant challenges for large-scale pre-training where computational budgets must be strictly managed.

In this paper, we first demonstrate that a fixed-threshold Top- p MoE yields only marginal gains over Top- k routing when activating a similar number of parameters. Furthermore, its performance and computational cost are highly sensitive to the selection of p and introduce uncontrolled sparsity, resulting in unstable computational costs. This observation motivates the development of a sparsity-controllable dynamic Top- p routing mechanism. The primary challenge lies in the fact that the probability threshold does not naturally receive gradients; it serves only to binarize the expert mask (0/1), so treating it as a standard learnable parameter is ineffective. To overcome this, we draw inspiration from Proportional–Integral (PI) control in classical control theory and treat the global sparsity as a target signal [1, 62]. We estimate the current activated-expert sparsity from the router and update the probability threshold via a PI controller. In doing so, we (i) render the threshold effectively learnable, (ii) maintain the overall activated-expert ratio close to a user-specified budget across tokens and layers, and (iii) realize a truly dynamic Top- p MoE with explicit sparsity control. To further enhance per-layer routing flexibility, we introduce a dynamic routing normalization mechanism. This rescales layer-wise routing logits, enabling different layers to adaptively learn distinct expert-routing patterns without violating the global probability threshold constraint.

We conduct extensive experiments on both Large Language Models (LLMs) for Natural Language Processing (NLP) and Diffusion Transformers (DiTs) for Computer Vision (CV). Across these settings, DTop- p consistently outperforms both Top- k and fixed-threshold Top- p baselines, while maintaining equivalent average FLOPs to Top- k MoE and ensuring precise control over the number of activated experts. We further investigate scaling behavior regarding expert granularity, expert capacity, model size, and dataset size, demonstrating that DTop- p maintains its performance advantage across diverse scaling regimes. Additionally, we analyze the distribution of activated experts to confirm that DTop- p strictly adheres to the compute budget while adaptively allocating experts across different tokens and layers. Finally, ablation studies covering the PI controller, dynamic routing normalization, architectural choices, and loss designs provide a holistic view of this dynamic, sparsity-controllable Top- p mechanism for large-scale pre-training.

Our main contributions are summarized as follows:

- ★ **Revisiting fixed-threshold Top- p MoE.** We demonstrate that existing Top- p routing with a global fixed probability threshold yields only limited gains over Top- k routing while remaining sensitive to the selection of p . Moreover, it produces uncontrolled and sometimes highly variable sparsity, which is undesirable for large-scale MoE pre-training.
- ★ **Sparsity-controllable dynamic Top- p MoE.** We propose DTop- p MoE, a dynamic Top- p routing scheme that renders the probability threshold effectively learnable via a PI controller. We additionally introduce dynamic routing normalization to enable adaptive layer-wise expert-selection diversity under a global probability threshold constraint.
- ★ **Comprehensive empirical validation.** On both NLP and CV benchmarks, DTop- p trains stronger MoE models than Top- k and fixed Top- p baselines while precisely controlling the sparsity level. Furthermore, our scaling investigations and ablations provide robust evidence and practical guidance for adopting DTop- p in large foundation models.

2 Preliminary Investigation

To investigate the efficacy of fixed-threshold Top- p MoE, we compare a Dense-1.3B model against an MoE-1.3B-6.9B-64E8A architecture (64 total experts, 8 activated per token, 6.9B total parameters, and 1.3B active parameters; see Table 1 for architecture details). Both models are trained on 100B tokens from the DCLM-Baseline dataset [30]. We evaluate the standard Top- k MoE against the Top- p MoE formulation using fixed thresholds of 0.30, 0.35, and 0.40 (see Section 3 for method introduction). All hyperparameters for both Top- k and Top- p MoE are optimized via grid search (see Appendix C for details). Figure 1 illustrates the training/validation/inference performance and

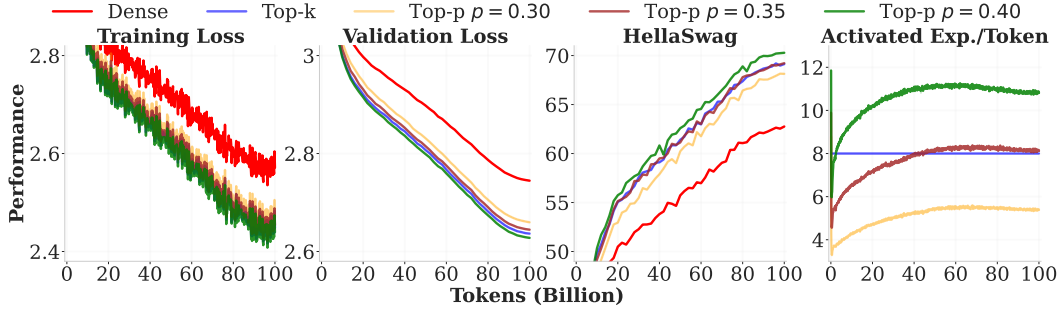


Figure 1: Performance comparison of the Dense model, Top- k MoE, and fixed-threshold Top- p MoE ($p \in \{0.30, 0.35, 0.40\}$). Top- p yields only marginal gains over Top- k MoE at comparable activation levels, while the number of activated experts fluctuates unpredictably throughout the training process.

the average number of activated experts per token in training batches (batch size $\approx 1\text{M}$ tokens). We observe that the number of activated experts in Top- p MoE fluctuates significantly, lacking a consistent trend. Initially, the count drops sharply, then gradually increases, eventually stabilizing near the end of training. This highlights a critical limitation of the current Top- p MoE: *sparsity levels are uncontrollable during training*. This unpredictability complicates resource allocation in practical scenarios, as the necessary computational budget is difficult to forecast. Regarding performance, Figure 1 shows that only Top- p MoE with a threshold of 0.40 slightly outperforms Top- k MoE; however, it activates over 12 experts for the majority of training. Conversely, with a threshold of 0.35, the model activates over 8 experts yet yields performance merely comparable to Top- k MoE. This suggests that fixed-threshold Top- p offers only marginal gains over Top- k MoE when activating a similar number of parameters. Furthermore, the drastic fluctuations in activated experts during training may induce performance degradation due to gradient instability [52]. Finally, Top- p MoE is highly sensitive to threshold selection. Determining an appropriate threshold requires extensive tuning; an ill-fitted threshold may trigger excessive expert activation in the final training stages, potentially causing Out-of-Memory (OOM) errors and wasting significant computational resources.

3 Method

To address the limitations of fixed-threshold Top- p MoE, we propose DTop- p MoE. This approach introduces a PI controller to maintain a target sparsity while employing dynamic routing normalization to adaptively adjust logit distributions across layers, thereby enabling distinctive sparsity patterns despite the use of a global probability threshold. We first introduce the concept of Top- k and Top- p MoE and then introduce DTop- p MoE. The overview of DTop- p MoE is shown in Figure 2.

3.1 Top- k and Top- p MoE

MoE architectures replace the standard dense feedforward layer in Transformer blocks with an MoE module. This module consists of a set of smaller feedforward networks (FFNs), referred to as experts [14, 29], and a router—a learned linear layer that maps input representations to specific experts. The output \mathbf{y} is computed as the weighted sum of the selected expert outputs:

$$\mathbf{y} = \sum_{i=1}^N r_i(\mathbf{x}) E_i(\mathbf{x}) \quad (1)$$

where \mathbf{x} represents the input token representation, N is the total number of experts, $E_i(\cdot)$ denotes the i -th expert network, and $r_i(\mathbf{x})$ is the routing probability assigned to expert i .

Given the router’s learnable weight matrix \mathbf{W} (omitting bias for simplicity), the initial expert probability distribution $\mathbf{P}(\mathbf{x})$ is computed via the softmax function:

$$\mathbf{P}(\mathbf{x}) = \text{softmax}(\mathbf{W}\mathbf{x}) \quad (2)$$

In **Top- k MoE** [14, 29], the routing mechanism selects a fixed number of k experts with the highest probability mass. Let σ be a permutation of indices $\{1, \dots, N\}$ that sorts the probabilities in

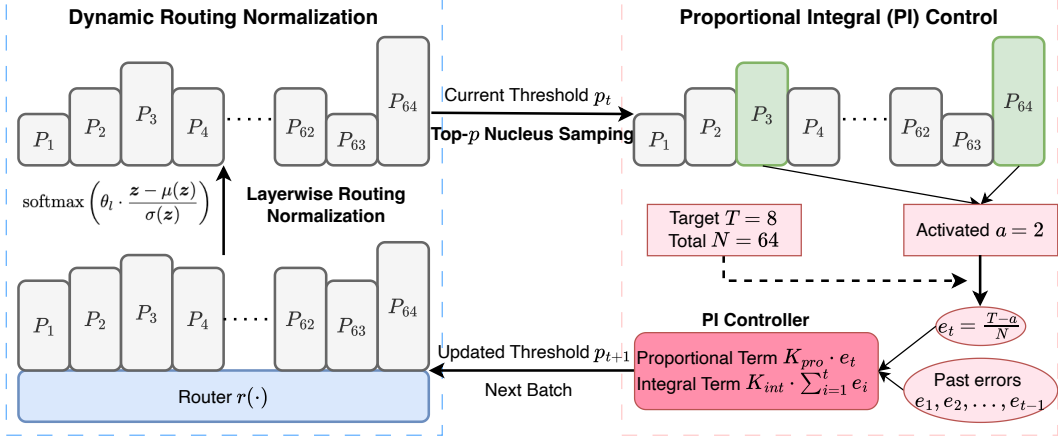


Figure 2: Overview of DTop- p MoE. We employ a Proportional-Integral (PI) controller to dynamically adjust the global probability threshold, aligning the number of activated experts with a target value. The Dynamic Routing Normalization modulates layer-wise logit distributions to support varying sparsity needs, enabling distinct patterns across network depths under the global threshold.

descending order, such that $P_{\sigma(1)}(\mathbf{x}) \geq P_{\sigma(2)}(\mathbf{x}) \geq \dots \geq P_{\sigma(N)}(\mathbf{x})$. The renormalized routing weights for Top- k MoE are defined as:

$$r_i(\mathbf{x}) = \begin{cases} \frac{P_i(\mathbf{x})}{\sum_{j=1}^k P_{\sigma(j)}(\mathbf{x})} & \text{if } i \in \{\sigma(1), \dots, \sigma(k)\}, \\ 0 & \text{otherwise} \end{cases} \quad (3)$$

In **Top- p MoE** [23, 55], which adopts the nucleus sampling mechanism [22], the router selects the smallest set of experts whose cumulative probability exceeds a threshold p . We define the dynamic cutoff index k_p as the minimum integer satisfying $\sum_{j=1}^{k_p} P_{\sigma(j)}(\mathbf{x}) \geq p$. Then the resulting routing probabilities for Top- p MoE are:

$$r_i(\mathbf{x}) = \begin{cases} \frac{P_i(\mathbf{x})}{\sum_{j=1}^{k_p} P_{\sigma(j)}(\mathbf{x})} & \text{if } i \in \{\sigma(1), \dots, \sigma(k_p)\}, \\ 0 & \text{otherwise} \end{cases} \quad (4)$$

3.2 Sparsity-Controllable Dynamic Top- p MoE

3.2.1 Proportional-Integral Control for Sparsity

As shown in Section 2, fixed-threshold Top- p MoE exhibits high computational variance and lacks the explicit resource constraints in Top- k methods. To address these limitations, we propose DTop- p MoE, which employs a feedback control mechanism to stabilize training. We model the number of activated experts as the process variable and the probability threshold as the control variable, using a PI controller to align the sparsity level with a specified target dynamically.

Formally, given a target number of activated experts T , we monitor the average number of activated experts per token, denoted as a_t , for the current batch \mathcal{B}_t . After computing the routing probabilities via Equation 4, the observed activation level is:

$$a_t = \frac{1}{M} \sum_{j=1}^M \sum_{i=1}^N \mathbb{1}(r_i(\mathbf{x}_j) > 0) \quad (5)$$

where M represents the total number of tokens in batch \mathcal{B}_t , N is the total number of experts, and $\mathbb{1}(\cdot)$ denotes the indicator function.

Because the threshold p is non-differentiable with respect to the routing decision, it cannot be optimized using gradient descent. Instead, we adjust p between steps to minimize the sparsity error defined as $e_t = (T - a_t)/N$. We apply a discrete PI control law to update the threshold p_{t+1} for the

subsequent batch:

$$p_{t+1} = p_0 + \underbrace{K_{pro} \cdot e_t}_{\text{Proportional}} + \underbrace{K_{int} \cdot \sum_{i=1}^t e_i}_{\text{Integral}} \quad (6)$$

where p_0 is the initial probability threshold, and K_{pro} and K_{int} are the proportional and integral gain coefficients, respectively.

This mechanism relies on the monotonicity of Nucleus Sampling [22]: increasing the cumulative probability threshold p strictly requires selecting more experts to satisfy the probability mass requirement. The PI controller uses this correlation to establish a negative feedback loop. A positive error (indicating insufficient activation) increases p , compelling the router to select more experts, whereas a negative error reduces p . The proportional term addresses immediate deviations, while the integral term accumulates past errors to eliminate steady-state bias [2]. This ensures the model converges to the target T even as the entropy of the logits shifts during training.

3.2.2 Dynamic Routing Normalization

Although the PI controller stabilizes global average sparsity, applying a single global threshold p_t across all layers assumes that expert confidence distributions are uniform throughout the network depth. However, deep networks often exhibit distinct sparsity requirements at different layers, such as broader processing in lower layers versus specialized processing in deeper layers [11, 24, 46]. Applying a global threshold to unnormalized logits may homogenize these patterns, potentially limiting representational capacity.

To address this issue, we introduce *Dynamic Routing Normalization*. Instead of routing directly on raw logits, we normalize the logits and apply a layer-specific learnable scale. This approach decouples the global threshold from the local statistical properties of the logits. For the l -th layer, the normalized routing probability is defined as:

$$P(\mathbf{x}) = \text{softmax} \left(\theta_l \cdot \frac{\mathbf{z} - \mu(\mathbf{z})}{\sigma(\mathbf{z})} \right), \quad \text{with } \mathbf{z} = \mathbf{W}\mathbf{x} \quad (7)$$

where \mathbf{z} denotes the raw logits, and $\mu(\mathbf{z})$ and $\sigma(\mathbf{z})$ represent their mean and standard deviation, respectively. The parameter θ_l is a learnable scalar for layer l that modulates the distribution temperature.

Optimizing θ_l allows the model to adaptively sharpen or flatten the probability distribution prior to applying the global threshold p_t . A larger θ_l results in a sharper distribution (activating fewer experts), whereas a smaller θ_l produces a flatter distribution (activating more experts). Consequently, DTop- p MoE maintains the global computational budget defined by the PI controller while enabling distinct sparsity patterns for each layer. The complete training procedure is provided in Algorithm 1 in Appendix B to facilitate a detailed understanding of the DTop- p MoE mechanism.

4 Experiments

In this section, we first outline our experimental setup, including model architectures, datasets, baselines, and hyperparameter configurations. We then evaluate DTop- p across two domains—NLP and CV—to demonstrate its improved performance over Top- k and fixed-threshold Top- p MoE, particularly regarding performance and precise sparsity control. Beyond establishing main results, we investigate the scaling properties of our method across expert granularity, expert capacity, model size, and training dataset size. Furthermore, we analyze the distribution of activated experts to validate the effectiveness of our sparsity control mechanism and to illustrate the adaptive allocation of experts across layers. Finally, comprehensive ablation studies examine the impact of the PI controller, Dynamic Routing Normalization, and various architectural and loss design choices.

4.1 Experimental Details

Models. For NLP tasks, our primary benchmarks utilize the Dense-1.3B and MoE-1.3B-6.9B-64E8A models. We further investigate the scaling performance using varying expert granularities,

Table 1: Architecture configurations for Dense and MoE variants (including Top- k , Top- p , and DTop- p settings) on NLP tasks. Additional configurations and hyperparameters are detailed in Tables 7 and 8 in Appendix C.

Setting	# Activated/Total Parameters	# Activated/Total Experts	# Layers	# Heads	# Dimension	# FFN Dimension
Dense-0.4B	0.4B/0.4B	1/1	16	16	1024	4096
Dense-1.3B	1.3B/1.3B	1/1	16	16	2048	8192
Dense-2.4B	2.4B/2.4B	1/1	32	32	2048	8192
MoE-0.4B-3.7B-64E8A	0.4B/3.7B	8/64	16	16	1024	512
MoE-1.3B-2.1B-16E8A	1.3B/2.1B	8/16	16	16	2048	1024
MoE-1.3B-3.7B-32E8A	1.3B/3.7B	8/32	16	16	2048	1024
MoE-1.3B-6.9B-32E4A	1.3B/6.9B	4/32	16	16	2048	2048
MoE-1.3B-6.9B-64E8A	1.3B/6.9B	8/64	16	16	2048	1024
MoE-1.3B-6.9B-128E16A	1.3B/6.9B	16/128	16	16	2048	512
MoE-2.4B-13.6B-64E8A	2.4B/13.6B	8/64	32	32	2048	1024

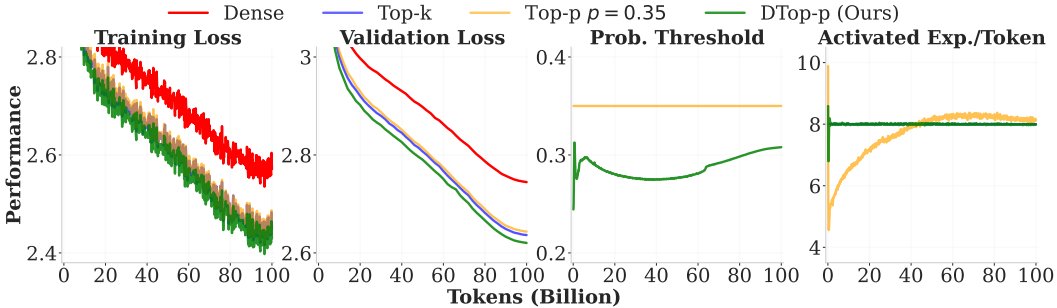


Figure 3: Training and validation performance of the Dense-1.3B and MoE-1.3B-6.9B-64E8A models using Top- k , Top- p , and DTop- p routing on NLP tasks. DTop- p achieves the best overall performance.

capacities, model sizes, and dataset sizes. The model architecture configurations for different settings are detailed in Table 1, with full hyperparameters provided in Table 7 and Table 8 in the Appendix. To validate DTop- p in the CV domain, we employ a DiT [44] featuring the 0.9B dense backbone and the 64E8A MoE variants (0.9B activated and 3.4B total parameters). Comprehensive architectural details are provided in Appendix C.

Datasets. For NLP, models are trained on DCLM-Baseline (DCLM) [30], a state-of-the-art open-source pre-training corpus filtered from Common Crawl. We train on 100B tokens for the main results and extend to 300B tokens for dataset scaling investigations. Following DCLM, we use the GPT-NeoX-20B [5] tokenizer with a sequence length of 2048. We monitor validation loss on C4 [13, 45] and, following prior works such as OLMoE [37] and OLMo [18], periodically probe in-training zero-shot performance on HellaSwag [57] and ARC-Easy [10]. After training evaluation spans **13 datasets** across five skill areas: commonsense reasoning, language understanding, reading comprehension, world knowledge, and symbolic problem solving. For CV, models are trained on 2 trillion pixel tokens comprising a mixture of high-quality internal images and image-text pairs. Performance is evaluated via validation loss on internal validation sets. Further details on training and evaluation datasets are provided in Appendix C and Appendix D.

Baselines. We compare DTop- p against three established baselines: (i) *Dense*: A standard dense model serving as a vanilla baseline; (ii) *Top- k* : The standard top- k routing MoE; and (iii) *Top- p* : A fixed probability threshold MoE with uncontrolled average expert activation. Note that for Top- k MoE, "activated experts" refers to the fixed count per token, whereas for Top- p and DTop- p MoE, it denotes the **target** number of activated experts for notational consistency.

Hyperparameters. We select hyperparameters either by following previous works [30, 37, 53] or by identifying optimal settings for each method via grid search. The detailed values used in our experiments are listed in Table 8 in Appendix C to ensure reproducibility.

Table 2: Inference performance comparison between Dense-1.3B and MoE-1.3B-6.9B-64E8A models with Top- k , Top- p , and DTop- p routing trained on 100B tokens. **Bold** indicates the best performance across all settings. Numbers in parentheses indicate the number of few-shot examples used in evaluation. DTop- p MoE achieves the highest average performance across the 13 benchmarks.

Area	Benchmark	Dense-1.3B	MoE-1.3B-6.9B-64E8A		
		Dense	Top- k	Top- p	DTop- p (Ours)
Symbolic Problem Solving	SVAMP(5)	5.3	10.3	8.3	16.0
	MMLU(5)	25.2	26.6	26.8	27.4
World Knowledge	ARC-Easy(0)	60.9	65.7	65.5	67.1
	ARC-Challenge(0)	34.4	40.6	40.9	41.7
Commonsense Reasoning	COPA(5)	69.0	82.0	82.0	85.0
	PIQA(5)	75.7	78.9	77.7	78.1
Language Understanding	HellaSwag(0)	62.7	69.1	69.2	70.9
	WinoGrande(5)	62.7	64.0	66.3	67.2
	LAMBADA(5)	56.7	61.5	63.5	62.5
Reading Comprehension	BoolQ(5)	55.4	63.9	63.9	65.4
	AGIEval-LSAT-RC(5)	26.2	22.7	23.8	27.2
	AGIEval-LSAT-LR(5)	26.0	26.4	24.9	25.5
	AGIEval-SAT-EN(5)	26.5	24.8	27.7	27.7
Average		45.1	49.0	49.3	50.9

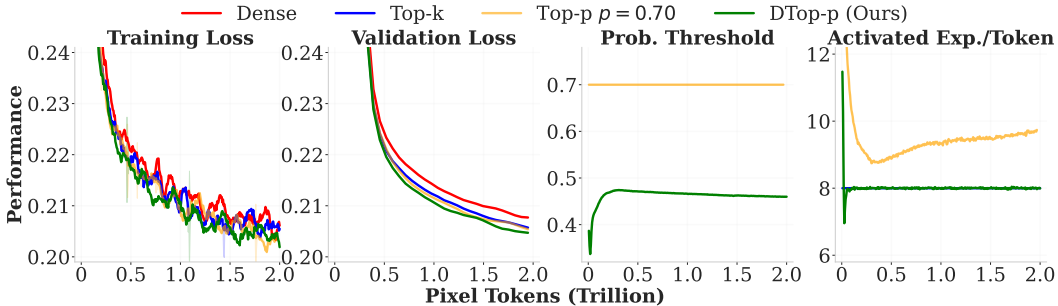


Figure 4: Training and validation performance of the 0.9B Dense model versus the 64E8A MoE model (0.9B activated / 3.4B total parameters) using Top- k , Top- p , and DTop- p routing on CV tasks. DTop- p achieves the best performance.

4.2 Main Results

NLP Results. We compare the performance of DTop- p against the Dense baseline, Top- k MoE, and fixed probability-threshold Top- p MoE on NLP tasks, while maintaining the average number of activated experts per token at the target level. Figure 3 illustrates the training and validation performance for the Dense-1.3B and MoE-1.3B-6.9B-64E8A models trained on 100B tokens. We observe that DTop- p improves training and validation performance compared to all baselines. Notably, although the fixed-threshold Top- p MoE activates more than 8 experts in the final training stages, it yields performance comparable to Top- k MoE. In contrast, DTop- p maintains precise control over the number of activated experts (targeting 8) via the proposed PI controller and Dynamic Routing Normalization, while outperforming Top- k MoE. This demonstrates the efficacy of our method regarding both performance and sparsity control.

Table 2 details the inference performance across 13 benchmarks. DTop- p achieves an average score improvement of 1.9 points compared to Top- k MoE, demonstrating the robustness and generalization capabilities of the method on complex real-world NLP tasks.

CV Results. To validate the cross-domain applicability of our method, we conduct experiments using DiTs on CV tasks. Figure 4 illustrates the training and validation performance of a 0.9B Dense baseline compared to a 64E8A MoE model (0.9B activated, 3.4B total parameters). These models are

Table 3: Performance comparison of Dense-1.3B vs. MoE-1.3B-6.9B models across varying expert granularities (32E4A, 64E8A, 128E16A) trained on 100B tokens. DTop- p is scalable with respect to expert granularity and consistently outperforms Dense and Top- k MoE baselines.

Area	Benchmark	Dense-1.3B	1.3B-6.9B-32E4A		1.3B-6.9B-64E8A		1.3B-6.9B-128E16A	
		Dense	Top- k	DTop- p	Top- k	DTop- p	Top- k	DTop- p
Symbolic Problem Solving	SVAMP(5)	5.3	11.6	11.0	10.3	16.0	11.6	15.0
	MMLU(5)	25.2	25.0	27.2	26.6	27.4	27.2	26.8
World Knowledge	ARC-Easy(0)	60.9	67.4	66.7	65.7	67.1	66.2	69.5
	ARC-Challenge(0)	34.4	39.8	40.9	40.6	41.7	38.9	42.5
Commonsense Reasoning	COPA(5)	69.0	78.0	82.0	82.0	85.0	82.0	88.0
	PIQA(5)	75.7	77.3	78.1	78.9	78.1	77.4	78.1
Language Understanding	HellaSwag(0)	62.7	68.6	69.9	69.1	70.9	69.1	71.3
	WinoGrande(5)	62.7	64.6	65.8	64.0	67.2	64.7	67.5
	LAMBADA(5)	56.7	62.2	63.1	61.5	62.5	62.1	64.6
Reading Comprehension	BoolQ(5)	55.4	61.0	63.7	63.9	65.4	63.9	65.2
	AGIEval-LSAT-RC(5)	26.2	24.2	26.2	22.7	27.2	24.6	26.2
	AGIEval-LSAT-LR(5)	26.0	23.3	25.3	26.4	25.5	26.0	25.9
	AGIEval-SAT-EN(5)	26.5	26.8	25.9	24.8	27.7	26.8	27.9
Average		45.1	48.4	49.7	49.0	50.9	49.3	51.4

Table 4: Inference performance of Dense-1.3B vs. MoE models with varying expert capacities (1.3B-2.1B-16E8A, 1.3B-3.7B-32E8A, 1.3B-6.9B-64E8A) trained on 100B tokens. DTop- p consistently achieves strong performance as total expert capacity increases.

Area	Benchmark	Dense-1.3B	1.3B-2.1B-16E8A		1.3B-3.7B-32E8A		1.3B-6.9B-64E8A	
		Dense	Top- k	DTop- p	Top- k	DTop- p	Top- k	DTop- p
Symbolic Problem Solving	SVAMP(5)	5.3	6.3	8.0	5.9	11.0	10.3	16.0
	MMLU(5)	25.2	24.8	25.8	26.7	26.7	26.6	27.4
World Knowledge	ARC-Easy(0)	60.9	62.9	64.7	65.0	66.8	65.7	67.1
	ARC-Challenge(0)	34.4	35.4	38.1	38.9	39.2	40.6	41.7
Commonsense Reasoning	COPA(5)	69.0	75.0	78.0	82.0	85.0	82.0	85.0
	PIQA(5)	75.7	76.4	76.1	77.4	77.7	78.9	78.1
Language Understanding	HellaSwag(0)	62.7	65.3	66.4	67.5	68.1	69.1	70.9
	WinoGrande(5)	62.7	64.4	64.6	65.9	66.3	64.0	67.2
	LAMBADA(5)	56.7	59.2	59.8	60.9	61.8	61.5	62.5
Reading Comprehension	BoolQ(5)	55.4	62.0	62.7	64.9	64.1	63.9	65.4
	AGIEval-LSAT-RC(5)	26.2	26.4	23.9	22.3	25.7	22.7	27.2
	AGIEval-LSAT-LR(5)	26.0	23.4	23.3	24.3	25.9	26.4	25.5
	AGIEval-SAT-EN(5)	26.5	23.3	23.3	23.3	23.8	24.8	27.7
Average		45.1	46.5	47.3	48.1	49.4	49.0	50.9

trained on 2 trillion pixel tokens using Top- k , Top- p , and DTop- p routing mechanisms. Consistent with our NLP findings, DTop- p outperforms both Top- k and the fixed-threshold Top- p baselines while successfully constraining the number of activated experts to the target level. This further demonstrates the effectiveness of our method on DiTs.

4.3 Scaling Performance

We examine the scaling properties of Dense, Top- k MoE, and DTop- p across four axes: expert granularity, total expert capacity, model size, and dataset size. We exclude fixed-threshold Top- p MoE from this analysis because dynamically tuning probability thresholds to maintain target activation sparsity across diverse configurations is computationally prohibitive. Furthermore, our earlier experiments indicate that Top- p MoE yields only marginal improvements over Top- k MoE when matched for activated parameters.

Scaling Expert Granularity. We evaluate the impact of expert granularity by fixing the total and activated parameter counts while varying the expert configuration (activated/total experts) from 4/32 to 8/64 and 16/128. The results in Table 3 demonstrate that: ❶ DTop- p scales effectively with granularity; performance consistently improves as the expert ratio shifts from 4/32 to 16/128. ❷ DTop- p consistently outperforms Top- k MoE across all granularities. ❸ DTop- p demonstrates higher

Table 5: Inference performance of Dense models vs. varying 64E8A MoE models across different model sizes (0.4B, 1.3B, 2.4B) trained on 100B tokens. DTop- p consistently achieves the best performance and scales effectively with model size.

Area	Benchmark	Dense-0.4B			MoE-0.4B-3.7B			Dense-1.3B			MoE-1.3B-6.9B			Dense-2.4B			MoE-2.4B-13.6B		
		Dense	Top- k	DTop- p	Dense	Top- k	DTop- p	Dense	Top- k	DTop- p	Dense	Top- k	DTop- p	Dense	Top- k	DTop- p	Dense	Top- k	DTop- p
<i>Symbolic Problem Solving</i>	SVAMP(5)	6.3	4.0	6.6	5.3	10.3	16.0	11.0	13.6	22.6									
<i>World Knowledge</i>	MMLU(5)	25.0	23.9	24.8	25.2	26.6	27.4	24.6	28.2	29.0									
	ARC-Easy(0)	52.9	61.3	62.1	60.9	65.7	67.1	64.7	70.2	70.7									
	ARC-Challenge(0)	26.9	32.5	33.7	34.4	40.6	41.7	37.7	45.5	44.6									
<i>Commonsense Reasoning</i>	COPA(5)	63.0	72.0	74.0	69.0	82.0	85.0	80.0	84.0	87.0									
	PIQA(5)	71.2	74.5	75.0	75.7	78.9	78.1	77.2	79.1	79.5									
<i>Language Understanding</i>	HellaSwag(0)	48.8	60.6	60.7	62.7	69.1	70.9	67.9	73.9	74.4									
	WinoGrande(5)	55.8	59.7	59.9	62.7	64.0	67.2	67.4	70.6	71.8									
	LAMBADA(5)	46.8	54.5	56.2	56.7	61.5	62.5	63.8	68.6	69.4									
<i>Reading Comprehension</i>	BoolQ(5)	58.9	62.4	64.1	55.4	63.9	65.4	69.2	68.0	71.2									
	AGIEval-LSAT-RC(5)	21.2	23.9	23.9	26.2	22.7	27.2	24.2	24.2	26.2									
	AGIEval-LSAT-LR(5)	24.5	22.1	23.5	26.0	26.4	25.5	24.5	22.1	26.1									
	AGIEval-SAT-EN(5)	23.7	22.3	23.3	26.5	24.8	27.7	27.6	27.7	30.5									
Average		40.4	44.1	45.2	45.1	49.0	50.9	49.2	52.0	54.1									

Table 6: Inference performance of Dense-1.3B vs. MoE-1.3B-6.9B-64E8A models trained on 100B tokens versus 300B tokens. DTop- p consistently achieves the best performance and scales effectively with training dataset size.

Area	Benchmark	Dense-1.3B (100B)			MoE-1.3B-6.9B (100B)			Dense-1.3B (300B)			MoE-1.3B-6.9B (300B)		
		Dense	Top- k	DTop- p	Dense	Top- k	DTop- p	Dense	Top- k	DTop- p	Dense	Top- k	DTop- p
<i>Symbolic Problem Solving</i>	SVAMP(5)	5.3	10.3	16.0	6.3	22.6	27.7						
<i>World Knowledge</i>	MMLU(5)	25.2	26.6	27.4	25.3	27.7	29.1						
	ARC-Easy(0)	60.9	65.7	67.1	64.2	70.5	71.2						
	ARC-Challenge(0)	34.4	40.6	41.7	37.4	44.1	45.3						
<i>Commonsense Reasoning</i>	COPA(5)	69.0	82.0	85.0	79.0	82.0	86.0						
	PIQA(5)	75.7	78.9	78.1	77.1	79.1	79.8						
<i>Language Understanding</i>	HellaSwag(0)	62.7	69.1	70.9	66.3	73.9	74.5						
	WinoGrande(5)	62.7	64.0	67.2	64.9	69.2	70.4						
	LAMBADA(5)	56.7	61.5	62.5	61.8	64.5	68.2						
<i>Reading Comprehension</i>	BoolQ(5)	55.4	63.9	65.4	66.4	70.5	71.9						
	AGIEval-LSAT-RC(5)	26.2	22.7	27.2	25.7	23.8	25.7						
	AGIEval-LSAT-LR(5)	26.0	26.4	25.5	23.9	22.1	24.9						
	AGIEval-SAT-EN(5)	26.5	24.8	27.7	28.6	25.2	25.2						
Average		45.1	49.0	50.9	48.2	51.9	53.8						

scaling efficiency than Top- k MoE, as the performance gap between the two methods widens at higher granularities.

Scaling Expert Capacity. Next, we analyze scaling behavior regarding expert capacity. We maintain a constant number of activated experts and activated parameters while increasing the total number of experts. As shown in Table 4: ❶ DTop- p benefits from increased capacity, with performance improving as the total number of experts increases. ❷ DTop- p consistently achieves superior performance compared to both Dense and Top- k MoE baselines across all capacity configurations.

Scaling Model Size. We assess scalability across model sizes by varying the number of layers, heads, and dimensions while maintaining a fixed expert granularity. The results in Table 5 reveal that: ❶ DTop- p scales robustly with model size, consistently achieving the best performance across the 0.4B, 1.3B, and 2.4B configurations. ❷ The performance advantage of DTop- p over Top- k MoE becomes more pronounced as model size increases, highlighting its superior scalability.

Scaling Dataset Size. Finally, we examine the effect of training duration by increasing the dataset size from 100B to 300B tokens while maintaining the same model architecture. The results in Table 6 indicate that: ❶ DTop- p exhibits strong data scaling properties, with performance improving significantly as the number of training tokens increases. ❷ DTop- p consistently outperforms the Dense and Top- k MoE counterparts at larger data scales, further validating the effectiveness of DTop- p MoE.

In summary, DTop- p demonstrates robust scalability across expert granularity, capacity, model size, and dataset size. It consistently outperforms Dense and Top- k MoE baselines, with the performance

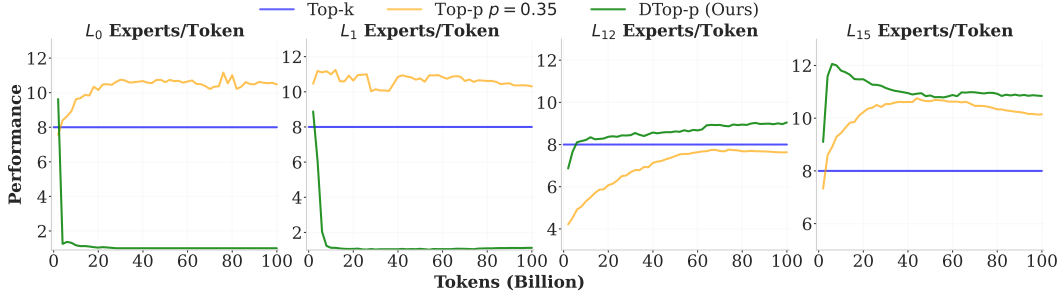


Figure 5: Layer-wise evolution of activated experts per token during training (MoE-1.3B-6.9B-64E8A, 100B tokens). We compare Top- k , Top- p , and DTop- p across 4 representative layers. DTop- p learns to activate fewer experts in shallow layers while utilizing more experts in deeper layers.

advantage becoming increasingly pronounced at higher granularities and larger model sizes. These results validate the efficacy of DTop- p for large-scale pre-training.

4.4 Activated Experts Distribution Analysis

Layer-wise Activated Experts Distribution. We analyze the distribution of activated experts across layers throughout the training process. Figure 5 illustrates the layer-wise activation dynamics for the MoE-1.3B-6.9B-64E8A model using Top- k , fixed-threshold Top- p , and DTop- p , trained on 100B tokens (showing four representative layers; see Figure 11 in Appendix E for full results). Our observations are as follows: ❶ In shallow layers ($L_0 - L_2$), the number of activated experts in DTop- p rapidly decreases to approximately 1, whereas fixed-threshold Top- p maintains a high activation count (≥ 8). Conversely, in deeper layers ($L_{12} - L_{15}$), DTop- p recruits more experts than both Top- k and Top- p . This observation is consistent with prior findings that shallow layers capture broad, general-purpose features (requiring fewer activations), while deep layers require high specialization for semantic reasoning [11, 46, 49]. This indicates that DTop- p effectively learns distinct, layer-adaptive sparsity patterns. ❷ Furthermore, DTop- p achieves convergence significantly faster than Top- p in the middle and deep layers, indicating improved stability in activation dynamics.

Training and Validation Activated Experts. We further analyze global activation statistics to validate the controllability of expert sparsity in DTop- p . Figure 6 presents the mean and standard deviation of activated experts per token on both training and validation sets. We observe that: ❶ DTop- p successfully maintains the average number of activated experts at the target value across both training and validation datasets, confirming the effectiveness of the sparsity control mechanism. ❷ The number of activated experts converges significantly faster when the PI controller is utilized in DTop- p , stabilizing within 1B tokens. In contrast, the activation count in Top- p converges only near the end of training as the learning rate decays. ❸ DTop- p exhibits a stable standard deviation (≈ 1), providing flexibility for tokens to activate varying numbers of experts while remaining significantly more stable than Top- p , which exhibits high variance (≈ 4).

4.5 Ablation Studies

Ablation of DTop- p Components. We isolate the contributions of the PI controller and Dynamic Routing Normalization (Dynamic RN) by conducting ablation experiments on the MoE-1.3B-6.9B-64E8A model trained on 30B tokens. We define three ablation settings: (1) *Top- p w/o both*: Corresponds to a standard fixed-threshold Top- p MoE ($p = 0.25$) utilizing fixed global routing logit normalization with a temperature of 1 [53]; (2) *Top- p w/o PI*: Utilizes Dynamic RN but relies on a fixed threshold ($p = 0.25$); and (3) *Top- p w/o Dynamic RN*: Employs the PI controller combined with fixed global routing logit normalization with a temperature of 1. The results, presented in Figure 7, indicate that: ❶ DTop- p achieves optimal performance when both the PI controller and Dynamic RN are utilized. ❷ The PI controller improves performance by strictly regulating the number of activated experts to the target level; without it, activation counts remain uncontrolled and tend to drift upward during the initial training stages. ❸ Dynamic RN further enhances performance by dynamically

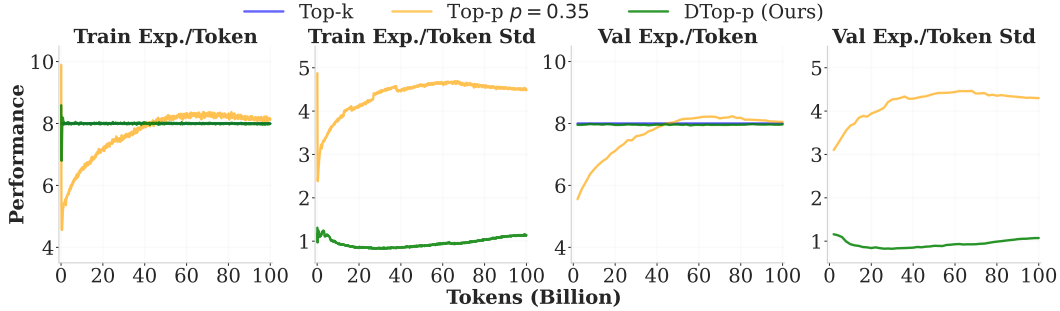


Figure 6: Mean and standard deviation of activated experts per token on training and validation sets for Top- k , Top- p , and DTop- p MoE. DTop- p effectively and rapidly converges to the target activation level on both training and validation datasets.

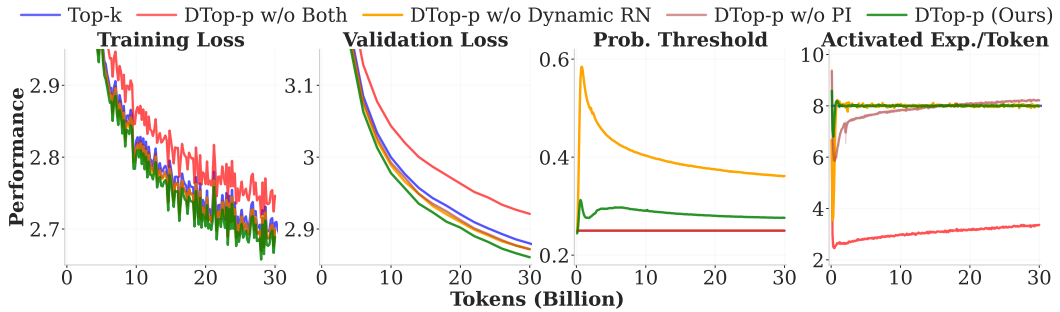


Figure 7: Ablation study of the PI controller (PI) and Dynamic Routing Normalization (Dynamic RN). DTop- p achieves the best performance when both components are combined.

adjusting layer-wise logit distributions. This adaptively stabilizes the probability threshold and routing behavior, mitigating the large threshold fluctuations observed when Dynamic RN is omitted.

We further compare DTop- p MoE with Top- k MoE combined with Dynamic RN in Figure 12 in Appendix E. We observe that: ❶ DTop- p MoE achieves better performance compared to Top- k MoE with Dynamic RN. ❷ Although Dynamic RN enhances the performance of Top- k MoE, it yields a significantly larger improvement in Top- p MoE. This suggests that Dynamic RN is more effective when the number of activated experts varies adaptively, rather than being constrained to a uniform k .

PI Controller Tuning. We investigate the sensitivity of the PI controller to its hyperparameters—specifically probability initialization, K_{pro} , and K_{int} —using the MoE-1.3B-6.9B-64E8A model trained on 20B tokens. The results are presented in Figure 8 (probability initialization) and Figure 9 (K_{pro} and K_{int}). We observe the following: ❶ DTop- p is robust to probability initialization values, as the PI controller rapidly aligns the number of activated experts with the target level under different initializations. This represents a significant advantage over fixed-threshold Top- p MoE, which is highly sensitive to initialization and requires extensive tuning to identify an appropriate probability threshold (as shown in Figure 1). ❷ The coefficients K_{pro} and K_{int} regulate convergence speed. Moderate values yield optimal performance, balancing the rapid convergence of activated experts with the stability of the probability threshold. Excessively large values induce threshold instability, negatively affecting loss, whereas very small values result in slow convergence.

Weight Tying. Weight tying shares parameters between the input token embedding layer and the final output projection layer, whereas untied approaches maintain distinct parameters for these components. To evaluate this technique, we conduct an ablation using the MoE-1.3B-6.9B-64E8A model trained on 30B tokens. As illustrated in Figure 10, weight tying significantly enhances the performance of DTop- p . This improvement is likely attributable to the implicit regularization provided by the reduced parameter count, which mitigates overfitting. Additionally, weight tying enforces a consistent geometric representation between the input and output embedding spaces, facilitating better convergence.

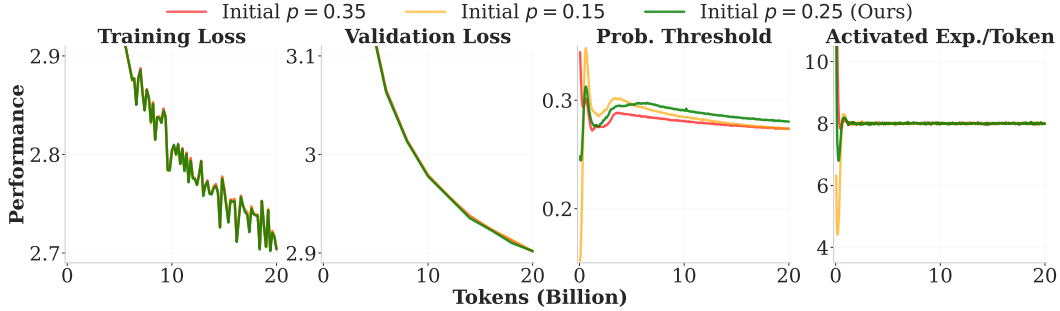


Figure 8: Performance of the PI controller across various probability initialization values. Unlike fixed-threshold methods, DTop- p is insensitive to initialization, consistently converging to optimal performance.

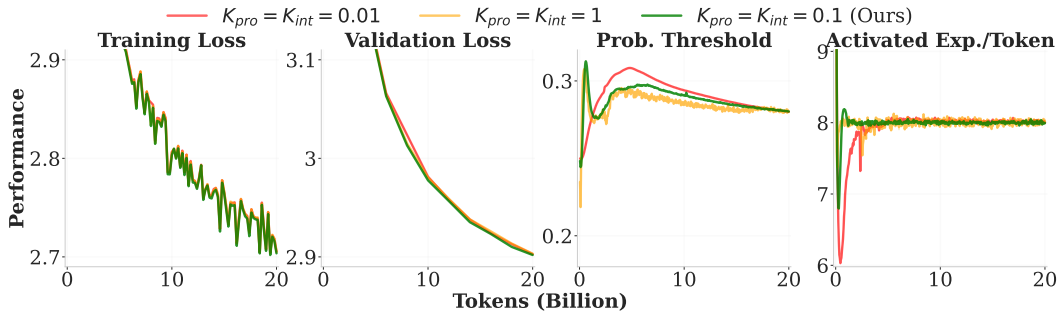


Figure 9: Performance of the PI controller across various K_{pro} and K_{int} values. DTop- p achieves the best performance with moderate PI coefficient values.

AdamW Optimizer Tuning. We conduct a comprehensive hyperparameter sweep for the AdamW optimizer, specifically analyzing the Learning Rate (LR), Weight Decay, and Epsilon. The performance for the MoE-1.3B-6.9B-64E8A model trained on 100B tokens are detailed in Appendix E (Figures 13, 14, and 15). Our findings indicate: **1 Learning Rate:** A moderate LR of $3e-3$ yields optimal performance. Excessively high LRs induce instability, evidenced by significant spikes in training loss, whereas smaller LRs lead to premature plateaus at higher loss levels, indicating a failure to fully traverse the loss landscape within the training budget. **2 Weight Decay:** A moderate Weight Decay of $3.3e-2$ proves most effective. Higher values appear to over-regularize the model, impeding the reduction of training loss. Conversely, insufficient weight decay (smaller values) results in sub-optimal convergence. **3 Epsilon:** Smaller Epsilon values ($1e-8$ and $1e-10$) consistently outperform larger ones for DTop- p . This aligns with observations in Top- k MoE models [37], suggesting that lower Epsilon values can maintain numerical stability and improve the optimizer’s adaptive properties when handling the dynamic routing distributions.

4.6 Loss Designs

To ensure training stability and routing efficiency in DTop- p , we optimize a composite objective function for NLP tasks comprising four distinct terms: Language Modeling Loss, Load Balancing Loss, Dynamic Loss, and Router Z-Loss. To determine the optimal configuration, we conduct comprehensive hyperparameter tuning using the MoE-1.3B-6.9B-64E8A model trained on 30B tokens. Results for these ablation studies are detailed in Appendix E (Figures 16, 17, 18, and 19).

Language Modeling Loss (LM Loss). Our primary optimization objective is the standard Cross-Entropy Loss, augmented with an auxiliary Z-Loss term [8] to enhance training stability. While the Cross-Entropy term minimizes the negative log-likelihood of the target tokens, the Z-Loss regularizes the partition function of the final softmax layer. This regularization mitigates "logit drift"—a phenomenon where the magnitude of output logits increases indefinitely, leading to numerical

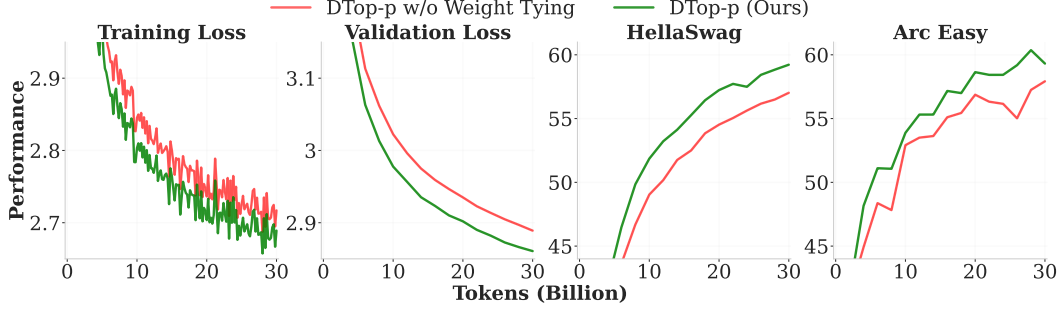


Figure 10: Ablation results for weight tying. The configuration with weight tying yields significantly better performance than the untied counterpart.

instability. The total language modeling loss is defined as:

$$L_{\text{LM}} = \frac{1}{M} \sum_{j=1}^M \left[\underbrace{-\log \frac{\exp(\mathbf{z}_{j,y_j})}{\sum_{v=1}^V \exp(\mathbf{z}_{j,v})}}_{\text{Cross-Entropy}} + \lambda_z \cdot \underbrace{\left(\log \sum_{v=1}^V \exp(\mathbf{z}_{j,v}) \right)^2}_{\text{Auxiliary Z-Loss}} \right] \quad (8)$$

where M is the batch size (in tokens), V is the vocabulary size, $\mathbf{z}_{j,v}$ denotes the output logit for the j -th token and vocabulary index v , y_j is the ground-truth token index, and λ_z is the LM Z-Loss coefficient.

Observation: As shown in Figure 16, the LM Z-Loss has a minor impact on DTop- p performance. A small coefficient of 1×10^{-4} yields the best results.

Load Balancing Loss (LB Loss). Widely adopted in sparse MoE architectures [29, 48], the Load Balancing Loss prevents the router from collapsing into a trivial solution where only a few experts are utilized. It encourages a uniform distribution of tokens across all experts. The loss is formulated as:

$$L_{\text{LB}} = \lambda_{\text{lbl}} \cdot N \cdot \sum_{i=1}^N f_i \cdot Q_i \quad (9)$$

where λ_{lbl} is the LB Loss coefficient and N is the number of experts. f_i denotes the fraction of tokens discretely dispatched to expert i , and Q_i represents the average probability mass allocated to expert i :

$$f_i = \frac{1}{M} \sum_{j=1}^M \mathbb{1}(r_i(\mathbf{x}_j) > 0), \quad Q_i = \frac{1}{M} \sum_{j=1}^M P_i(\mathbf{x}_j) \quad (10)$$

Here, \mathbf{x}_j is the input representation for the j -th token, and $\mathbb{1}(\cdot)$ is the indicator function.

Observation: As shown in Figure 17, a small coefficient of 1×10^{-4} achieves optimal performance. Larger coefficients degrade performance, likely because excessive weight on auxiliary balancing constraints interferes with the primary optimization of model weights.

Dynamic Loss. To encourage decisiveness in the router, we employ the Dynamic Loss [23]. This objective minimizes the entropy of the routing distribution, thereby compelling the router to assign high probabilities to a small, decisive set of experts (sharpening the distribution) rather than spreading probability mass uniformly. It is defined as:

$$L_{\text{Dynamic}} = -\lambda_{\text{dl}} \cdot \frac{1}{M} \sum_{j=1}^M \sum_{i=1}^N P_i(\mathbf{x}_j) \cdot \log(P_i(\mathbf{x}_j)) \quad (11)$$

where λ_{dl} is the Dynamic Loss coefficient.

Observation: As shown in Figure 18, a moderate coefficient of 1×10^{-3} achieves the best performance. Larger coefficients negatively impact results by making the routing distribution excessively sharp, which increases the probability threshold too aggressively and hinders exploration.

Router Z-Loss. Finally, to ensure numerical stability within the MoE layers, we adopt the Router Z-Loss introduced in ST-MoE [63]. Large input logits can cause numeric overflow during the large-scale matrix multiplications characteristic of MoE layers. The Router Z-Loss penalizes large logit magnitudes:

$$L_{\text{Router-Z}} = \lambda_{rz} \cdot \frac{1}{M} \sum_{j=1}^M \left(\log \sum_{i=1}^N \exp(\mathbf{W}_i \cdot \mathbf{x}_j^T) \right)^2 \quad (12)$$

where λ_{rz} is the Router Z-Loss coefficient and $\mathbf{W}_i \cdot \mathbf{x}_j^T$ represents the pre-softmax logit for the i -th expert.

Observation: As shown in Figure 19, Router Z-Loss proves counter-productive for DTop- p . Increasing the coefficient causes the probability threshold to drop dramatically, indicating that Router Z-Loss forces the routing distribution to become flatter. This flattening prevents experts from learning distinct, specialized knowledge [23, 53]. Consequently, we set $\lambda_{rz} = 0$.

5 Conclusion

In this work, we introduce DTop- p , a novel dynamic routing mechanism designed to overcome the limitations of Top- k routing and the instability of fixed-threshold Top- p approaches. By integrating a PI controller with Dynamic Routing Normalization, DTop- p achieves precise, stable control over the number of activated experts while allowing for dynamic token and layer level adaptability. Our extensive empirical evaluation demonstrates that DTop- p consistently outperforms Dense, Top- k , and fixed-threshold Top- p baselines across both Natural Language Processing and Computer Vision domains. Beyond standard benchmarks, we established that DTop- p exhibits better scaling properties with respect to expert granularity, total expert capacity, model size, and dataset size. Notably, our analysis of activation patterns reveals that DTop- p autonomously learns distinct layer-wise sparsity profiles—utilizing fewer experts for broad, general-purpose processing in shallow layers and recruiting more experts in deeper layers. These findings suggest that control-theoretic approaches can effectively stabilize dynamic routing in MoE architectures without sacrificing performance or computational efficiency. We hope DTop- p serves as a robust foundation for future research into adaptive computation and scalable sparse MoE.

References

- [1] Karl J Astrom. Pid controllers: theory, design, and tuning. *The international society of measurement and control*, 1995.
- [2] Karl Johan Åström and Richard Murray. *Feedback systems: an introduction for scientists and engineers*. Princeton university press, 2021.
- [3] Shuai Bai, Keqin Chen, Xuejing Liu, Jialin Wang, Wenbin Ge, Sibao Song, Kai Dang, Peng Wang, Shijie Wang, Jun Tang, Humen Zhong, Yuanzhi Zhu, Mingkun Yang, Zhaohai Li, Jianqiang Wan, Pengfei Wang, Wei Ding, Zheren Fu, Yiheng Xu, Jiabo Ye, Xi Zhang, Tianbao Xie, Zesen Cheng, Hang Zhang, Zhibo Yang, Haiyang Xu, and Junyang Lin. Qwen2.5-v1 technical report. *arXiv preprint arXiv:2502.13923*, 2025.
- [4] Yonatan Bisk, Rowan Zellers, Jianfeng Gao, Yejin Choi, et al. Piqa: Reasoning about physical commonsense in natural language. In *Proceedings of the AAAI conference on artificial intelligence*, volume 34, pages 7432–7439, 2020.
- [5] Sidney Black, Stella Biderman, Eric Hallahan, Quentin Anthony, Leo Gao, Laurence Golding, Horace He, Connor Leahy, Kyle McDonell, Jason Phang, et al. Gpt-neox-20b: An open-source autoregressive language model. In *Proceedings of BigScience Episode# 5–Workshop on Challenges & Perspectives in Creating Large Language Models*, pages 95–136, 2022.
- [6] Tom Brown, Benjamin Mann, Nick Ryder, Melanie Subbiah, Jared D Kaplan, Prafulla Dhariwal, Arvind Neelakantan, Pranav Shyam, Girish Sastry, Amanda Askell, et al. Language models are few-shot learners. *Advances in neural information processing systems*, 33:1877–1901, 2020.

- [7] Chengkun Cai, Xu Zhao, Haoliang Liu, Zhongyu Jiang, Tianfang Zhang, Zongkai Wu, Jenq-Neng Hwang, and Lei Li. The role of deductive and inductive reasoning in large language models. In *Proceedings of the 63rd Annual Meeting of the Association for Computational Linguistics (Volume 1: Long Papers)*, pages 16780–16790, 2025.
- [8] Aakanksha Chowdhery, Sharan Narang, Jacob Devlin, Maarten Bosma, Gaurav Mishra, Adam Roberts, Paul Barham, Hyung Won Chung, Charles Sutton, Sebastian Gehrmann, et al. Palm: Scaling language modeling with pathways. *Journal of Machine Learning Research*, 24(240): 1–113, 2023.
- [9] Christopher Clark, Kenton Lee, Ming-Wei Chang, Tom Kwiatkowski, Michael Collins, and Kristina Toutanova. Boolq: Exploring the surprising difficulty of natural yes/no questions. In *Proceedings of the 2019 Conference of the North American Chapter of the Association for Computational Linguistics: Human Language Technologies, Volume 1 (Long and Short Papers)*, pages 2924–2936, 2019.
- [10] Peter Clark, Isaac Cowhey, Oren Etzioni, Tushar Khot, Ashish Sabharwal, Carissa Schoenick, and Oyvind Tafjord. Think you have solved question answering? try arc, the ai2 reasoning challenge. *arXiv preprint arXiv:1803.05457*, 2018.
- [11] Damai Dai, Li Dong, Yaru Hao, Zhifang Sui, Baobao Chang, and Furu Wei. Knowledge neurons in pretrained transformers. In *Proceedings of the 60th Annual Meeting of the Association for Computational Linguistics (Volume 1: Long Papers)*, pages 8493–8502, 2022.
- [12] Damai Dai, Chengqi Deng, Chenggang Zhao, Rx Xu, Huazuo Gao, Deli Chen, Jiashi Li, Wangding Zeng, Xingkai Yu, Y Wu, et al. Deepseekmoe: Towards ultimate expert specialization in mixture-of-experts language models. In *Proceedings of the 62nd Annual Meeting of the Association for Computational Linguistics (Volume 1: Long Papers)*, pages 1280–1297, 2024.
- [13] Jesse Dodge, Maarten Sap, Ana Marasović, William Agnew, Gabriel Ilharco, Dirk Groeneveld, Margaret Mitchell, and Matt Gardner. Documenting large webtext corpora: A case study on the colossal clean crawled corpus. In *Proceedings of the 2021 Conference on Empirical Methods in Natural Language Processing*, pages 1286–1305, 2021.
- [14] William Fedus, Barret Zoph, and Noam Shazeer. Switch transformers: Scaling to trillion parameter models with simple and efficient sparsity. *Journal of Machine Learning Research*, 23(120):1–39, 2022.
- [15] Trevor Gale, Deepak Narayanan, Cliff Young, and Matei Zaharia. Megablocks: Efficient sparse training with mixture-of-experts. *Proceedings of Machine Learning and Systems*, 5:288–304, 2023.
- [16] Andrew Gordon, Zornitsa Kozareva, and Melissa Roemmele. SemEval-2012 task 7: Choice of plausible alternatives: An evaluation of commonsense causal reasoning. In Eneko Agirre, Johan Bos, Mona Diab, Suresh Manandhar, Yuval Marton, and Deniz Yuret, editors, **SEM 2012: The First Joint Conference on Lexical and Computational Semantics – Volume 1: Proceedings of the main conference and the shared task, and Volume 2: Proceedings of the Sixth International Workshop on Semantic Evaluation (SemEval 2012)*, pages 394–398, Montréal, Canada, 7-8 June 2012. Association for Computational Linguistics. URL <https://aclanthology.org/S12-1052/>.
- [17] Aaron Grattafiori, Abhimanyu Dubey, Abhinav Jauhri, Abhinav Pandey, Abhishek Kadian, Ahmad Al-Dahle, Aiesha Letman, Akhil Mathur, Alan Schelten, Alex Vaughan, et al. The llama 3 herd of models. *arXiv preprint arXiv:2407.21783*, 2024.
- [18] Dirk Groeneveld, Iz Beltagy, Evan Walsh, Akshita Bhagia, Rodney Kinney, Oyvind Tafjord, Ananya Jha, Hamish Ivison, Ian Magnusson, Yizhong Wang, et al. Olmo: Accelerating the science of language models. In *Proceedings of the 62nd Annual Meeting of the Association for Computational Linguistics (Volume 1: Long Papers)*, pages 15789–15809, 2024.
- [19] Daya Guo, Dejian Yang, Haowei Zhang, Junxiao Song, Ruoyu Zhang, Runxin Xu, Qihao Zhu, Shirong Ma, Peiyi Wang, Xiao Bi, et al. Deepseek-r1: Incentivizing reasoning capability in llms via reinforcement learning. *arXiv preprint arXiv:2501.12948*, 2025.

- [20] Yongxin Guo, Zhenglin Cheng, Xiaoying Tang, Zhaopeng Tu, and Tao Lin. Dynamic mixture of experts: An auto-tuning approach for efficient transformer models. *arXiv preprint arXiv:2405.14297*, 2024.
- [21] Dan Hendrycks, Collin Burns, Steven Basart, Andy Zou, Mantas Mazeika, Dawn Song, and Jacob Steinhardt. Measuring massive multitask language understanding. In *International Conference on Learning Representations*, 2021.
- [22] Ari Holtzman, Jan Buys, Li Du, Maxwell Forbes, and Yejin Choi. The curious case of neural text degeneration. *arXiv preprint arXiv:1904.09751*, 2019.
- [23] Quzhe Huang, Zhenwei An, Nan Zhuang, Mingxu Tao, Chen Zhang, Yang Jin, Kun Xu, Liwei Chen, Songfang Huang, and Yansong Feng. Harder tasks need more experts: Dynamic routing in moe models. *arXiv preprint arXiv:2403.07652*, 2024.
- [24] Ganesh Jawahar, Benoît Sagot, and Djamel Seddah. What does bert learn about the structure of language? In *ACL 2019-57th Annual Meeting of the Association for Computational Linguistics*, 2019.
- [25] Can Jin, Tong Che, Hongwu Peng, Yiyuan Li, Dimitris Metaxas, and Marco Pavone. Learning from teaching regularization: Generalizable correlations should be easy to imitate. *Advances in Neural Information Processing Systems*, 37:966–994, 2024.
- [26] Can Jin, Yang Zhou, Qixin Zhang, Hongwu Peng, Di Zhang, Marco Pavone, Ligong Han, Zhang-Wei Hong, Tong Che, and Dimitris N Metaxas. Your reward function for rl is your best prm for search: Unifying rl and search-based tts. *arXiv preprint arXiv:2508.14313*, 2025.
- [27] Peng Jin, Bo Zhu, Li Yuan, and Shuicheng Yan. Moe++: Accelerating mixture-of-experts methods with zero-computation experts. *arXiv preprint arXiv:2410.07348*, 2024.
- [28] Jared Kaplan, Sam McCandlish, Tom Henighan, Tom B Brown, Benjamin Chess, Rewon Child, Scott Gray, Alec Radford, Jeffrey Wu, and Dario Amodei. Scaling laws for neural language models. *arXiv preprint arXiv:2001.08361*, 2020.
- [29] Dmitry Lepikhin, HyoukJoong Lee, Yuanzhong Xu, Dehao Chen, Orhan Firat, Yanping Huang, Maxim Krikun, Noam Shazeer, and Zhifeng Chen. Gshard: Scaling giant models with conditional computation and automatic sharding. *arXiv preprint arXiv:2006.16668*, 2020.
- [30] Jeffrey Li, Alex Fang, Georgios Smyrnis, Maor Ivgi, Matt Jordan, Samir Yitzhak Gadre, Hritik Bansal, Etash Guha, Sedrick Scott Keh, Kushal Arora, et al. Datacomp-lm: In search of the next generation of training sets for language models. *Advances in Neural Information Processing Systems*, 37:14200–14282, 2024.
- [31] Lei Li, Sen Jia, Jianhao Wang, Zhongyu Jiang, Feng Zhou, Ju Dai, Tianfang Zhang, Zongkai Wu, and Jenq-Neng Hwang. Human motion instruction tuning. In *Proceedings of the Computer Vision and Pattern Recognition Conference*, pages 17582–17591, 2025.
- [32] Aixin Liu, Bei Feng, Bing Xue, Bingxuan Wang, Bochao Wu, Chengda Lu, Chenggang Zhao, Chengqi Deng, Chenyu Zhang, Chong Ruan, et al. Deepseek-v3 technical report. *arXiv preprint arXiv:2412.19437*, 2024.
- [33] Shicheng Liu and Minghui Zhu. Distributed inverse constrained reinforcement learning for multi-agent systems. *Advances in Neural Information Processing Systems*, 35:33444–33456, 2022.
- [34] Shicheng Liu and Minghui Zhu. Learning multi-agent behaviors from distributed and streaming demonstrations. *Advances in Neural Information Processing Systems*, 36:53552–53564, 2023.
- [35] Shicheng Liu and Minghui Zhu. Meta inverse constrained reinforcement learning: Convergence guarantee and generalization analysis. *International Conference on Learning Representations*, 2024.

- [36] Jan Ludziejewski, Jakub Krajewski, Kamil Adamczewski, Maciej Pióro, Michał Krutul, Szymon Antoniak, Kamil Ciebiera, Krystian Król, Tomasz Odrzygóźdź, Piotr Sankowski, et al. Scaling laws for fine-grained mixture of experts. In *Forty-first International Conference on Machine Learning*, 2024.
- [37] Niklas Muennighoff, Luca Soldaini, Dirk Groeneveld, Kyle Lo, Jacob Morrison, Sewon Min, Weijia Shi, Evan Pete Walsh, Oyvind Tafjord, Nathan Lambert, et al. Olmoe: Open mixture-of-experts language models. In *The Thirteenth International Conference on Learning Representations*, 2025.
- [38] OpenAI. Learning to reason with llms, September 2024. URL <https://openai.com/index/learning-to-reason-with-llms/>.
- [39] OpenAI. Gpt-4o system card. Technical report, OpenAI, August 2024. URL <https://cdn.openai.com/gpt-4o-system-card.pdf>.
- [40] OpenAI. gpt-oss-120b and gpt-oss-20b model card, 2025. URL <https://arxiv.org/abs/2508.10925>.
- [41] Long Ouyang, Jeffrey Wu, Xu Jiang, Diogo Almeida, Carroll Wainwright, Pamela Mishkin, Chong Zhang, Sandhini Agarwal, Katarina Slama, Alex Ray, et al. Training language models to follow instructions with human feedback. *Advances in neural information processing systems*, 35:27730–27744, 2022.
- [42] Denis Paperno, Germán Kruszewski, Angeliki Lazaridou, Ngoc Quan Pham, Raffaella Bernardi, Sandro Pezzelle, Marco Baroni, Gemma Boleda, and Raquel Fernández. The LAMBADA dataset: Word prediction requiring a broad discourse context. In Katrin Erk and Noah A. Smith, editors, *Proceedings of the 54th Annual Meeting of the Association for Computational Linguistics (Volume 1: Long Papers)*, pages 1525–1534, Berlin, Germany, August 2016. Association for Computational Linguistics. doi: 10.18653/v1/P16-1144. URL <https://aclanthology.org/P16-1144/>.
- [43] Arkil Patel, Satwik Bhattamishra, and Navin Goyal. Are NLP models really able to solve simple math word problems? In Kristina Toutanova, Anna Rumshisky, Luke Zettlemoyer, Dilek Hakkani-Tur, Iz Beltagy, Steven Bethard, Ryan Cotterell, Tanmoy Chakraborty, and Yichao Zhou, editors, *Proceedings of the 2021 Conference of the North American Chapter of the Association for Computational Linguistics: Human Language Technologies*, pages 2080–2094, Online, June 2021. Association for Computational Linguistics. doi: 10.18653/v1/2021.naacl-main.168. URL <https://aclanthology.org/2021.naacl-main.168/>.
- [44] William Peebles and Saining Xie. Scalable diffusion models with transformers. In *Proceedings of the IEEE/CVF international conference on computer vision*, pages 4195–4205, 2023.
- [45] Colin Raffel, Noam Shazeer, Adam Roberts, Katherine Lee, Sharan Narang, Michael Matena, Yanqi Zhou, Wei Li, and Peter J Liu. Exploring the limits of transfer learning with a unified text-to-text transformer. *Journal of machine learning research*, 21(140):1–67, 2020.
- [46] Carlos Riquelme, Joan Puigcerver, Basil Mustafa, Maxim Neumann, Rodolphe Jenatton, André Susano Pinto, Daniel Keysers, and Neil Houlsby. Scaling vision with sparse mixture of experts. *Advances in Neural Information Processing Systems*, 34:8583–8595, 2021.
- [47] Keisuke Sakaguchi, Ronan Le Bras, Chandra Bhagavatula, and Yejin Choi. Winogrande: An adversarial winograd schema challenge at scale. *Communications of the ACM*, 64(9):99–106, 2021.
- [48] Noam Shazeer, Azalia Mirhoseini, Krzysztof Maziarz, Andy Davis, Quoc Le, Geoffrey Hinton, and Jeff Dean. Outrageously large neural networks: The sparsely-gated mixture-of-experts layer. *arXiv preprint arXiv:1701.06538*, 2017.
- [49] Yehui Tang, Yichun Yin, Yaoyuan Wang, Hang Zhou, Yu Pan, Wei Guo, Ziyang Zhang, Miao Rang, Fangcheng Liu, Naifu Zhang, et al. Pangu ultra moe: How to train your big moe on ascend npus. *arXiv preprint arXiv:2505.04519*, 2025.

- [50] Kimi Team, Yifan Bai, Yiping Bao, Guanduo Chen, Jiahao Chen, Ningxin Chen, Ruijie Chen, Yanru Chen, Yuankun Chen, Yutian Chen, et al. Kimi k2: Open agentic intelligence. *arXiv preprint arXiv:2507.20534*, 2025.
- [51] The Mosaic ML Team. composer. <https://github.com/mosaicml/composer/>, 2021.
- [52] Ziteng Wang, Jun Zhu, and Jianfei Chen. Remoe: Fully differentiable mixture-of-experts with relu routing. *arXiv preprint arXiv:2412.14711*, 2024.
- [53] Tianwen Wei, Bo Zhu, Liang Zhao, Cheng Cheng, Biye Li, Weiwei Lü, Peng Cheng, Jianhao Zhang, Xiaoyu Zhang, Liang Zeng, et al. Skywork-moe: A deep dive into training techniques for mixture-of-experts language models. *arXiv preprint arXiv:2406.06563*, 2024.
- [54] An Yang, Anfeng Li, Baosong Yang, Beichen Zhang, Binyuan Hui, Bo Zheng, Bowen Yu, Chang Gao, Chengen Huang, Chenxu Lv, et al. Qwen3 technical report. *arXiv preprint arXiv:2505.09388*, 2025.
- [55] Yuanhang Yang, Shiyi Qi, Wenchao Gu, Chaozheng Wang, Cuiyun Gao, and Zenglin Xu. Xmoe: Sparse models with fine-grained and adaptive expert selection. *arXiv preprint arXiv:2403.18926*, 2024.
- [56] Ziyu Yao, Xuxin Cheng, Zhiqi Huang, and Lei Li. Countllm: Towards generalizable repetitive action counting via large language model. In *Proceedings of the Computer Vision and Pattern Recognition Conference*, pages 19143–19153, 2025.
- [57] Rowan Zellers, Ari Holtzman, Yonatan Bisk, Ali Farhadi, and Yejin Choi. Hellaswag: Can a machine really finish your sentence? In *Proceedings of the 57th Annual Meeting of the Association for Computational Linguistics*, pages 4791–4800, 2019.
- [58] Wanjun Zhong, Ruixiang Cui, Yiduo Guo, Yaobo Liang, Shuai Lu, Yanlin Wang, Amin Saied, Weizhu Chen, and Nan Duan. AGIEval: A human-centric benchmark for evaluating foundation models. In Kevin Duh, Helena Gomez, and Steven Bethard, editors, *Findings of the Association for Computational Linguistics: NAACL 2024*, pages 2299–2314, Mexico City, Mexico, June 2024. Association for Computational Linguistics. doi: 10.18653/v1/2024.findings-naacl.149. URL <https://aclanthology.org/2024.findings-naacl.149/>.
- [59] Yang Zhou, Mingyu Zhao, Zhenting Wang, Difei Gu, Bangwei Guo, Ruosong Ye, Ligong Han, Can Jin, and Dimitris N Metaxas. M3-bench: Multi-modal, multi-hop, multi-threaded tool-using mllm agent benchmark. *arXiv preprint arXiv:2511.17729*, 2025.
- [60] Yang Zhou, Shiyu Zhao, Yuxiao Chen, Zhenting Wang, Can Jin, and Dimitris N Metaxas. Led: Llm enhanced open-vocabulary object detection without human curated data generation. *arXiv preprint arXiv:2503.13794*, 2025.
- [61] Yanqi Zhou, Tao Lei, Hanxiao Liu, Nan Du, Yanping Huang, Vincent Zhao, Andrew M Dai, Quoc V Le, James Laudon, et al. Mixture-of-experts with expert choice routing. *Advances in Neural Information Processing Systems*, 35:7103–7114, 2022.
- [62] John G Ziegler and Nathaniel B Nichols. Optimum settings for automatic controllers. *Transactions of the American society of mechanical engineers*, 64(8):759–765, 1942.
- [63] Barret Zoph, Irwan Bello, Sameer Kumar, Nan Du, Yanping Huang, Jeff Dean, Noam Shazeer, and William Fedus. St-moe: Designing stable and transferable sparse expert models. *arXiv preprint arXiv:2202.08906*, 2022.

Appendix Contents

A Related Works	20
B Algorithm	20
C Training Details	20
D NLP Tasks Evaluation Details	21
E Additional Investigations and Ablation Studies	23
F Limitations	24
G Reproducibility Statement	25
H Ethics and Societal Impact	26

A Related Works

Mixture-of-Experts. Mixture-of-Experts (MoE) traces back to work in the early 1990s as a way to decompose a task into multiple specialized experts coordinated by a router. Shazeer et al. [48] introduce a sparse MoE layer between LSTM blocks and report strong results on language modeling and machine translation. Fedus et al. [14], Lepikhin et al. [29] integrate sparse MoE into Transformers and adopt a Top- k routing strategy for expert selection. As model scale grows, MoE becomes a prevailing approach for increasing capacity in foundation models without increasing activated computation [3, 19, 54]. Several works focus on making expert selection more fine-grained or more stable [12, 29], on analyzing and improving scaling behavior of MoE models [36], and on improving training efficiency through better systems and kernels [15, 29]. Another active line studies alternative routing mechanisms beyond fixed Top- k [20, 23, 27, 37, 52, 53, 55, 61]. Zhou et al. [61] study expert choice instead of token choice. Jin et al. [27] explore adding zero-compute experts to MoE. Guo et al. [20], Wang et al. [52] develop dynamic or differentiable routing to adapt expert assignment to the input. Huang et al. [23], Yang et al. [55] investigate accumulative Top- p routing with a fixed probability threshold. Our work stays closest to this dynamic/Top- p group, but introduces a *sparsity-controllable* dynamic Top- p MoE: we make the probability threshold effectively learnable via a PI controller and pair it with a dynamic gating normalization mechanism so that layers can adaptively learn different routing patterns under a single global sparsity budget.

Large Foundation Models. Large foundation models (LFMs) show strong generality across NLP, CV, and multimodal tasks [3, 19, 25, 26, 32–35, 38, 39, 44, 59, 60], mainly because model size and data size continue to scale. Dense LLMs with billions of parameters already reach competitive performance on many benchmarks [6, 7, 17, 31, 41, 54, 56]. At the same time, MoE-based LFMs become the dominant design in frontier systems [19, 32, 40, 50, 54], since they match or surpass dense models at similar activated compute and keep improving when model size, data size, expert granularity, and expert capacity increase [36, 37].

B Algorithm

Algorithm 1 outlines the training procedure for DTop- p . During the forward pass, the router first applies Dynamic Routing Normalization (Equation 7) to adaptively scale the logits within each layer. Subsequently, experts are selected via nucleus sampling based on the current global probability threshold p_t . To maintain the computational budget, the PI controller acts as a feedback mechanism: it monitors the deviation between the actual average number of activated experts a_t and the target T . This sparsity error is used to update the threshold p_{t+1} for the next step, leveraging proportional and integral terms to ensure the sparsity level converges stably to the target. Finally, all model parameters are optimized via gradient descent.

C Training Details

NLP Tasks. The main results utilize the Dense-1.3B and MoE-1.3B-6.9B-64E8A models trained on 100B DCLM-Baseline tokens. Architecture configurations are detailed in Tables 1 and 7, with method-specific hyperparameters provided in Table 8. In all experiments, we employ high expert granularity (e.g., 64E8A) rather than limited sets (e.g., 4E1A or 8E1A) to maximize the efficacy of the MoE architecture [12, 36]. Scaling performance investigations use the main hyperparameters unless otherwise specified. For ablation studies, we vary only the specific parameter under investigation relative to the DTop- p main hyperparameters listed in Table 8. We use the DCLM-Baseline dataset [30], a filtered subset of Common Crawl containing 3.8T tokens, from which we randomly sample 20B to 300B tokens for our experiments. We utilize the GPT-NeoX-20B [5] tokenizer with a sequence length of 2048. Due to resource constraints, most ablation experiments are conducted on 30B tokens. Validation is performed on the C4 validation set. All experiments are conducted using 64 or 128 NVIDIA A100 80GB GPUs.

CV Tasks. We employ a DiT-style denoiser comprising 28 layers, a hidden size of 2048, and 16 attention heads. Training utilizes the AdamW optimizer with a learning rate of 1×10^{-4} and weight decay of 0.01. We apply a Load Balancing (LB) Loss coefficient of 1×10^{-6} and a Dynamic Loss coefficient of 1×10^{-5} , omitting the Router Z-loss as it proves less critical for DiT pre-training. We

Algorithm 1 DTop- p MoE

Require: Dataset \mathcal{D} , target expert T , initial probability threshold p_0 , PI gain coefficient K_{pro}, K_{int} , model parameters Θ (including dynamic scales $\{\theta_l\}_{l=1}^L$)

- 1: Initialize integral error accumulation $e_{sum} \leftarrow 0$
- 2: Initialize probability threshold $p_1 = p_0$
- 3: **for** step $t = 1, 2, \dots$ with batch $\mathcal{B}_t \in \mathcal{D}$ **do**
- 4: Accumulator for number of activated experts $a_{sum} \leftarrow 0$
- 5: **Forward Pass:**
- 6: **for** layer $l = 1$ to L **do**
- 7: Compute raw logits for input representation \mathbf{x} : $\mathbf{z} \leftarrow \mathbf{W}\mathbf{x}$
- 8: **Dynamic Routing Normalization** (Equation 7): $\mathbf{P} \leftarrow \text{softmax}\left(\theta_l \cdot \frac{\mathbf{z} - \mu(\mathbf{z})}{\sigma(\mathbf{z})}\right)$
- 9: **Nucleus Sampling** with global threshold p_t :
- 10: Select minimal set of experts S such that $\sum_{i \in S} P_i \geq p_t$
- 11: $r_i(\mathbf{x}) \leftarrow \frac{P_i}{\sum_{j \in S} P_j}$ for $i \in S$, else 0 (Equation 4)
- 12: Record number of activated experts: $a_{sum} \leftarrow a_{sum} + |S|$
- 13: Compute layer output: $\mathbf{y} \leftarrow \sum_{i \in S} r_i(\mathbf{x}) E_i(\mathbf{x})$
- 14: **end for**
- 15: **PI controller Update** (Equation 6):
- 16: Calculate average activation per token: $a_t \leftarrow a_{sum} / (L \cdot |\mathcal{B}_t|)$, $|\mathcal{B}_t|$ is total tokens in \mathcal{B}_t
- 17: Calculate sparsity error: $e_t \leftarrow (T - a_t) / N$
- 18: Update integral term: $e_{sum} \leftarrow e_{sum} + e_t$
- 19: Update global threshold:
- 20: $p_{t+1} \leftarrow p_0 + K_{pro} \cdot e_t + K_{int} \cdot e_{sum}$
- 21: Clip p_{t+1} to range $(0, 1)$
- 22: **Optimization:**
- 23: Compute Total Loss \mathcal{L}
- 24: Update parameters Θ via gradient decent
- 25: **end for**

set the PI controller initial probability to 0.40; the Dynamic Routing Normalization and other PI controller hyperparameters match those used in the NLP experiments. Models are trained on 2 trillion pixel tokens aggregated from high-quality internal image datasets and image-text pairs. Performance is evaluated via validation loss on the internal validation set. All experiments are conducted using 64 NVIDIA A100 80GB GPUs.

Table 7: Architecture configurations for the Dense and MoE models on NLP tasks.

Architecture	Dense	MoE
Activation	SwiGLU	SwiGLU
Vocab size	50,432	50,432
LayerNorm type	Low-precision LayerNorm [51]	Low-precision LayerNorm
LayerNorm ϵ	1×10^{-5}	1×10^{-5}
QK-Norm	Yes	Yes
Position embedding	RoPE	RoPE
Biases	–	–
Weight tying	Yes	Yes
Init distribution	Truncated normal	Truncated normal
Init std	0.02	0.02
Init truncation	$3 \times \text{std}$	$3 \times \text{std}$
MoE layers	Every	Every

D NLP Tasks Evaluation Details

Setup. During pre-training, we monitor validation loss on C4 [13, 45] and, following prior work such as DataComp-LM [30], OLMoE [37], and OLMo [18], periodically probe **zero-shot** in-training

Table 8: Training hyperparameters for Dense, Top- k MoE, Top- p MoE, and DTop- p MoE on NLP tasks (“-” indicates not used/applicable).

Hyperparameters	Dense	Top- k MoE	Top- p MoE	DTop- p MoE
Sequence Length	2,048	2,048	2,048	2,048
Batch Size (Samples)	512	512	512	512
Batch Size (Tokens)	~1M	~1M	~1M	~1M
Warmup Steps	2,500	2,500	2,500	2,500
Peak LR	3.0E-3	3.0E-3	3.0E-3	3.0E-3
Minimum LR	3.0E-5	3.0E-5	3.0E-5	3.0E-5
Optimizer	AdamW	AdamW	AdamW	AdamW
Weight Decay	3.3E-2	3.3E-2	3.3E-2	3.3E-2
Beta1	0.9	0.9	0.9	0.9
Beta2	0.95	0.95	0.95	0.95
AdamW Epsilon	1.0E-8	1.0E-8	1.0E-8	1.0E-8
LR Schedule	Cosine	Cosine	Cosine	Cosine
Gradient Clipping	Global 1.0	Global 1.0	Global 1.0	Global 1.0
Gradient Reduce Dtype	FP32	FP32	FP32	FP32
Optimizer State Dtype	FP32	FP32	FP32	FP32
LM Z-loss Coefficient λ_z	1.0E-4	1.0E-4	1.0E-4	1.0E-4
LB Loss Coefficient λ_{lbt}	-	1.0E-4	1.0E-4	1.0E-4
Dynamic Loss Coefficient λ_{dl}	-	-	1.0E-3	1.0E-3
Router Z-loss Coefficient λ_{rz}	-	0	0	0
Probability Threshold Init.	-	-	0.25/0.30/0.35/0.40	0.25
Routing Normalization θ_t	-	Global 1.0 [53]	Global 1.0	Layer-wise Dynamic
PI K_{pro} Coefficient	-	-	-	0.1
PI K_{int} Coefficient	-	-	-	0.1

performance on HellaSwag [57] and ARC-Easy [10]. After pre-training, we conduct a comprehensive evaluation on **13 datasets** spanning five skill areas: commonsense reasoning, language understanding, reading comprehension, world knowledge, and symbolic problem solving. Unless otherwise specified, multiple-choice tasks are reported with **accuracy** (Acc.); the random baseline is 25% for four-choice and 50% for two-choice. For free-response tasks we report **exact match** (EM). Final evaluations use a **0/5-shot** setting with the standard community splits (see Table 9 for more details).

World Knowledge. This field probes encyclopedic and academic knowledge across the sciences, mathematics, social sciences, and humanities; items resemble standardized exams with carefully designed distractors.

- **MMLU** [21] (2019; 14,042 items; 4-choice): 57 subjects (e.g., jurisprudence, mathematics, ethics). Given a question and four options, the model outputs A/B/C/D. Metric: Acc.; random baseline **25%**.
- **ARC-Easy** [10] (2019; 2,376 items; 4-choice): Grade 3–9 science questions emphasizing basic scientific knowledge. Metric: Acc.; random baseline **25%**.
- **ARC-Challenge** [10] (2019; 1,172 items; 4-choice): The harder ARC subset requiring non-trivial science knowledge and procedural reasoning. Metric: Acc.; random baseline **25%**.

Symbolic Problem Solving. Benchmarks discrete, symbolic reasoning such as arithmetic and algebraic manipulation.

- **SVAMP** [43] (2023; 300 problems; free-response): Short grade-school arithmetic word problems with numerical answers. We prompt for chain-of-thought before the final answer and score with EM. Random baseline **0%**.

Commonsense Reasoning. Evaluates everyday causal and physical knowledge needed to select plausible outcomes.

- **COPA** [16] (2011; 100 items; 2-choice): Given a premise, choose the more plausible cause or effect. Metric: Acc.; random baseline **50%**.

Table 9: Evaluation suites and settings used during and after pre-training for NLP tasks.

Stage	Field	Dataset	Split	# Samples	Shot	Metric	Random Acc.
<i>During Pre-training</i>	Language Understanding	HellaSwag [57]	val	10,042	0	Multiple Choice Acc.	25%
	World Knowledge	ARC-Easy [10]	test	2,376	0	Multiple Choice Acc.	25%
<i>After Pre-training</i>	World Knowledge	MMLU [21]	test	14,042	5	Multiple Choice Acc.	25%
	World Knowledge	ARC-Easy [10]	test	2,376	0	Multiple Choice Acc.	25%
	World Knowledge	ARC-Challenge [10]	test	1,172	0	Multiple Choice Acc.	25%
	Symbolic Problem Solving	SVAMP [43]	test	300	5	Exact Match Acc.	0%
	Commonsense Reasoning	COPA [16]	val	100	5	Multiple Choice Acc.	50%
	Commonsense Reasoning	PIQA [4]	val	1,838	5	Multiple Choice Acc.	50%
	Language Understanding	HellaSwag [57]	val	10,042	0	Multiple Choice Acc.	25%
	Language Understanding	WinoGrande [47]	val	1,267	5	Cloze Formulation Acc.	50%
	Language Understanding	LAMBADA [42]	test	5,153	5	Language Modeling Acc.	0%
	Reading Comprehension	BoolQ [9]	val	3,270	5	Multiple Choice Acc.	50%
	Reading Comprehension	AGIEval-LSAT-RC [58]	test	268	5	Multiple Choice Acc.	25%
	Reading Comprehension	AGIEval-LSAT-LR [58]	test	510	5	Multiple Choice Acc.	25%
Reading Comprehension	AGIEval-SAT-EN [58]	test	206	5	Multiple Choice Acc.	25%	

- **PIQA** [4] (2019; 1,838 items; 2-choice): Physical commonsense—select the more sensible solution to a basic task. Metric: Acc.; random baseline **50%**.

Language Understanding. Assesses discourse coherence, referential consistency, and general linguistic regularities.

- **HellaSwag** [57] (2019; 10,042 items; 4-choice): Given a partial narrative, choose the most likely continuation. Metric: Acc.; random baseline **25%**.
- **WinoGrande** [47] (2012; 1,267 items; 2-choice): Large-scale coreference challenge—fill a blank with one of two candidates so the sentence is semantically valid. Metric: Acc.; random baseline **50%**.
- **LAMBADA** [42] (2016; 5,153 passages; LM/EM): Read a passage and predict its final token; scored with EM. Random baseline **0%**.

Reading Comprehension. Tests whether a model can answer questions using information explicitly or implicitly present in a passage.

- **BoolQ** [9] (2019; 3,270 items; yes/no): Short passages followed by binary questions. Metric: Acc.; random baseline **50%**.
- **AGIEval-LSAT-RC** [58] (2023; 268 items; 4-choice): LSAT Reading Comprehension—extract and integrate factual information from passages. Metric: Acc.; random baseline **25%**.
- **AGIEval-LSAT-LR** [58] (2023; 510 items; 4-choice): LSAT Logical Reasoning—draw conclusions and identify assumptions from short arguments. Metric: Acc.; random baseline **25%**.
- **AGIEval-SAT-EN** [58] (2023; 206 items; 4-choice): SAT-style English questions targeting high-school level reading and grammar. Metric: Acc.; random baseline **25%**.

E Additional Investigations and Ablation Studies

Layer-wise Activated Experts Distribution. The full results for layer-wise expert activation across all 16 layers are presented in Figure 11. These comprehensive plots corroborate the findings discussed in Section 4.4: $\text{DTop-}p$ consistently adopts a hierarchical sparsity strategy. Specifically, the model assigns minimal computational resources (nearing a single expert) to early layers ($L_0 - L_2$) to handle generic inputs, while allocating a larger expert budget to deeper layers ($L_{12} - L_{15}$) to manage complex semantic specializations.

Ablation of $\text{DTop-}p$ Components. Figure 12 presents the ablation results for $\text{Top-}k$, $\text{Top-}k$ with Dynamic Routing Normalization (DRN), $\text{DTop-}p$, and $\text{DTop-}p$ variants (without the PI controller, without DRN, and without both). We observe that $\text{DTop-}p$ achieves optimal performance when both

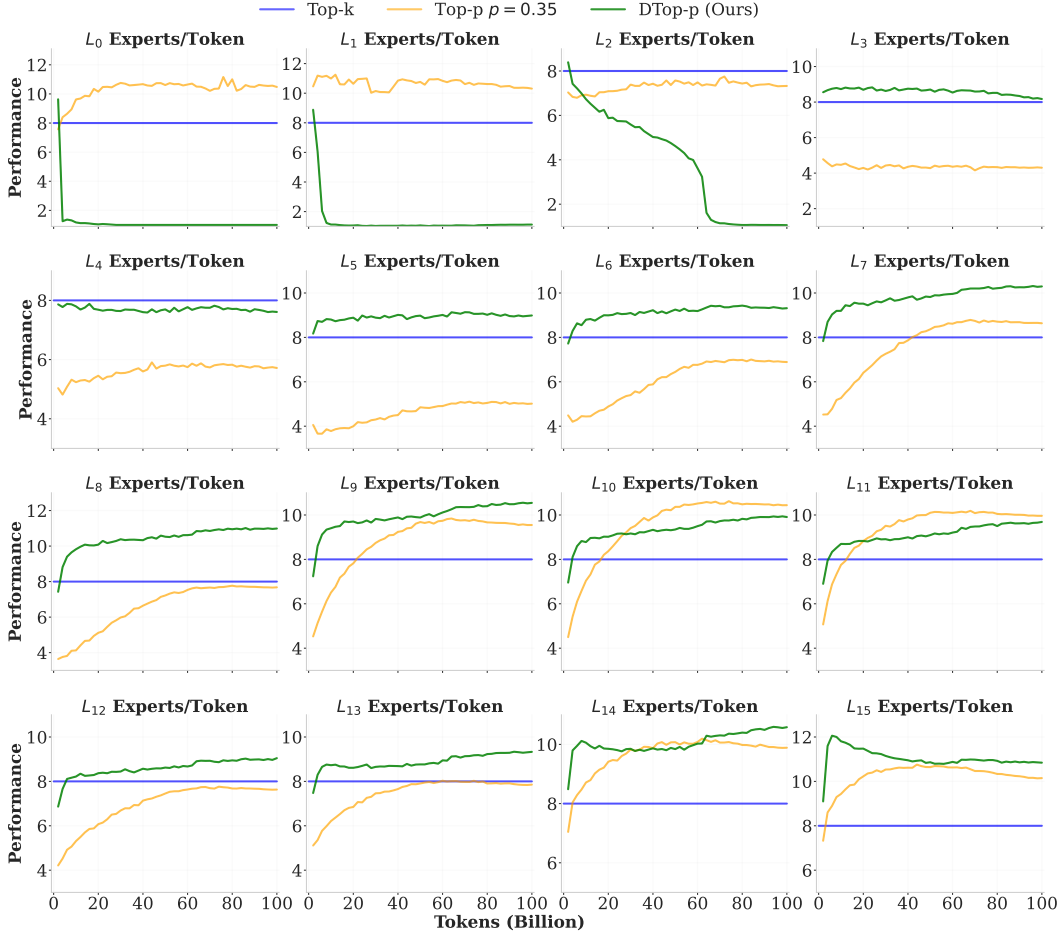


Figure 11: Comprehensive layer-wise evolution of activated experts per token for the MoE-1.3B-6.9B-64E8A model (100B tokens) across all 16 layers. DTop- p learns to activate fewer experts in shallow layers while utilizing more experts in deeper layers.

the PI controller and DRN are utilized. Furthermore, DTop- p outperforms Top- k paired with DRN, demonstrating the effectiveness of the combined PI controller and DRN mechanisms.

Hyperparameter Tuning of the AdamW Optimizer. We present the ablation results for the AdamW optimizer hyperparameters using the MoE-1.3B-6.9B-64E8A model trained on 100B tokens. Figures 13, 14, and 15 illustrate the impact of Learning Rate, Weight Decay, and Epsilon, respectively. The optimal configuration consists of a Learning Rate of $3e-3$, a Weight Decay of $3.3e-2$, and small Epsilon values ($1e-8$ or $1e-10$).

Hyperparameter Tuning of Loss Design. We present the hyperparameter tuning results for the Language Modeling Z-Loss, Load Balancing Loss, Dynamic Loss, and Router Z-Loss using the MoE-1.3B-6.9B-64E8A model trained on 30B tokens. The results are illustrated in Figures 18, 17, 19, and 16, respectively. Based on these experiments, the optimal coefficients for DTop- p are: LM Z-Loss $\lambda_z = 1 \times 10^{-4}$, Load Balancing Loss $\lambda_{lbl} = 1 \times 10^{-4}$, Dynamic Loss $\lambda_{dl} = 1 \times 10^{-3}$, and Router Z-Loss $\lambda_{rz} = 0$.

F Limitations

While DTop- p demonstrates superior performance and sparsity control compared to standard Top- k and fixed-threshold Top- p routing, several limitations remain. First, due to computational resource constraints, our scaling investigations are limited to models with a maximum of 13.6B total parameters

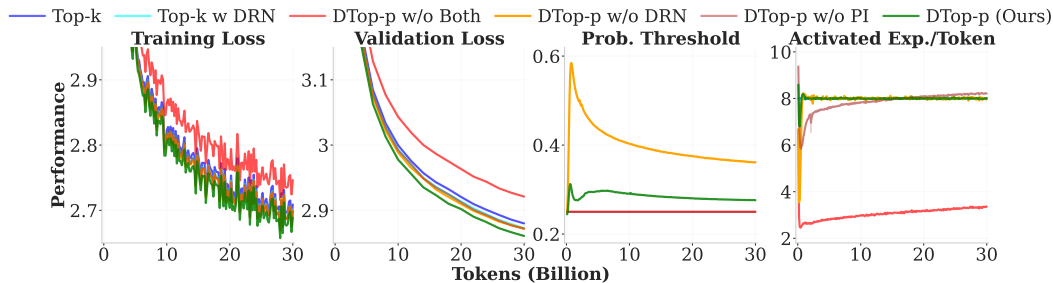


Figure 12: Ablation study of the PI controller (PI) and Dynamic Routing Normalization (DRN). DTop- p achieves optimal performance when both components are combined, surpassing Top- k with DRN.

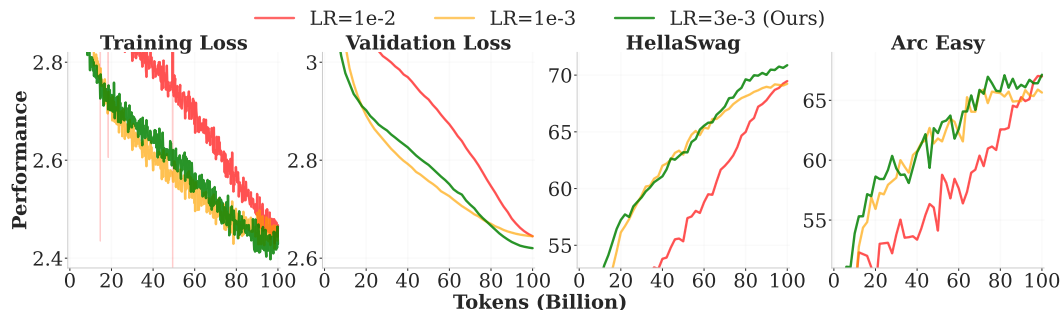


Figure 13: AdamW Learning Rate tuning results. A moderate Learning Rate of 3e-3 achieves the best performance, striking a balance between stability and convergence speed.

and training runs up to 300B tokens. While we observe consistent scaling laws within this regime, validating the effectiveness of DTop- p on frontier-scale foundation models (e.g., exceeding 100B active parameters or training on trillion-token corpora) remains future work. Second, although the PI controller proves robust to initialization in our experiments, it may require calibration when shifting to significantly different architectures or modalities outside of NLP and CV. Finally, our current implementation focuses on applying DTop- p to the router; the interaction between dynamic sparsity control and other advanced MoE techniques, such as expert-choice routing [61] or heterogeneous expert architectures [27] are not explored.

G Reproducibility Statement

We are committed to ensuring the reproducibility of our results. To this end, we provide the following resources:

- **Code and Data:** We will release the full source code for DTop- p , including the PI controller implementation, dynamic routing normalization, and training scripts, upon publication. All NLP datasets used in this work are either open-source or described with sufficient detail in Section 4.1 and Appendix C and D to allow reconstruction using comparable public data.
- **Algorithm Details:** The complete training procedure is formally described in Algorithm 1.
- **Hyperparameters:** We provide comprehensive tables of hyperparameters for all reported models. Table 1 and 7 detail the model architectures, while Table 8 in Appendix C lists the exact training configurations, including learning rates, batch sizes, optimizer settings, and loss coefficients.
- **Ablation Studies:** The specific hyperparameter ranges and configurations for our ablation studies (PI controller coefficients, loss coefficients, etc.) are detailed in the Figures in Section 4.5 and Appendix E to facilitate verification of our design choices.

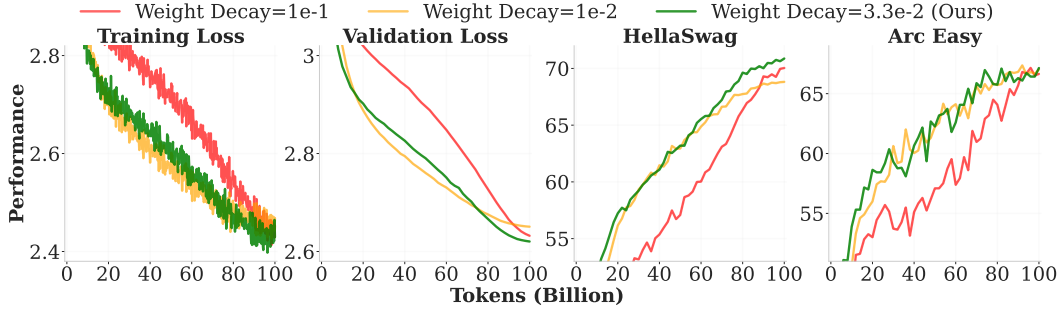


Figure 14: AdamW Weight Decay tuning results. A moderate Weight Decay of $3.3e-2$ achieves the best performance, avoiding both over-regularization and suboptimal convergence.

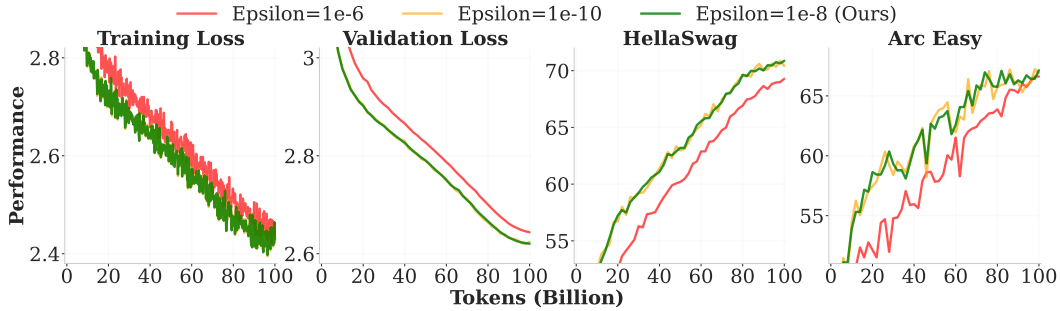


Figure 15: AdamW Epsilon tuning results. Smaller Epsilon values ($1e-8$ and $1e-10$) yield superior performance compared to larger values.

H Ethics and Societal Impact

The development of Large Foundation Models (LFMs) carries significant societal implications. We analyze the impact of our work from three primary perspectives:

Environmental Impact and Efficiency. Large-scale pre-training consumes substantial energy and contributes to carbon emissions. $D_{\text{Top-}p}$ addresses this challenge by improving the training efficiency of sparse MoE models. By enabling precise control over the number of activated experts, our method allows practitioners to strictly enforce computational budgets without the "sparsity drift" often seen in standard $\text{Top-}p$ methods. This capability potentially reduces the FLOPs required to reach a specific performance threshold, contributing to the broader goal of Green AI and sustainable model development.

Dataset Bias and Safety. Our NLP models are trained on the DCLM-Baseline dataset, which is derived from Common Crawl. Like all models trained on internet-scale text, our models may inherit biases, stereotypes, or toxic content present in the training data. While $D_{\text{Top-}p}$ improves the model's ability to select experts for processing information, it does not inherently filter or mitigate these data-centric issues. We strongly recommend that any deployment of models based on this architecture be preceded by rigorous safety alignment and red-teaming to mitigate potential harms.

Dual-Use Risks. As with any advancement in generative AI, the performance improvements enabled by $D_{\text{Top-}p}$ could theoretically be applied to generate harmful content, misinformation, or deepfakes. However, the technique itself is a general-purpose architectural improvement rather than a task-specific capability. We believe the benefits of efficient, scalable, and controllable computation outweigh the marginal increase in risk associated with general performance gains.

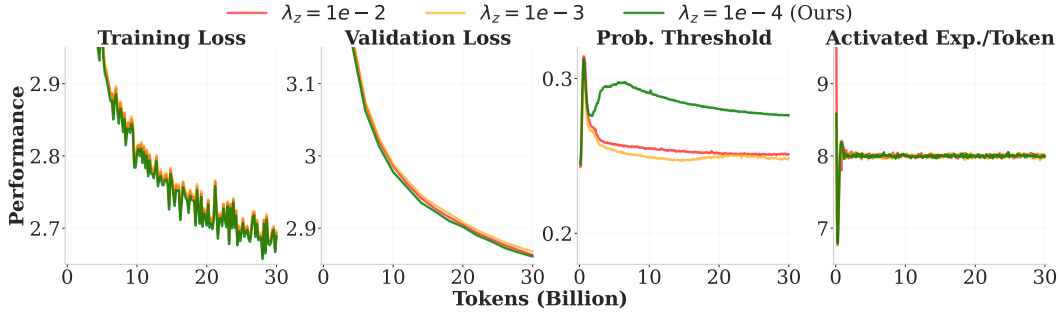


Figure 16: Language Modeling Z-Loss coefficient tuning results. A small coefficient of 1×10^{-4} achieves the best performance.

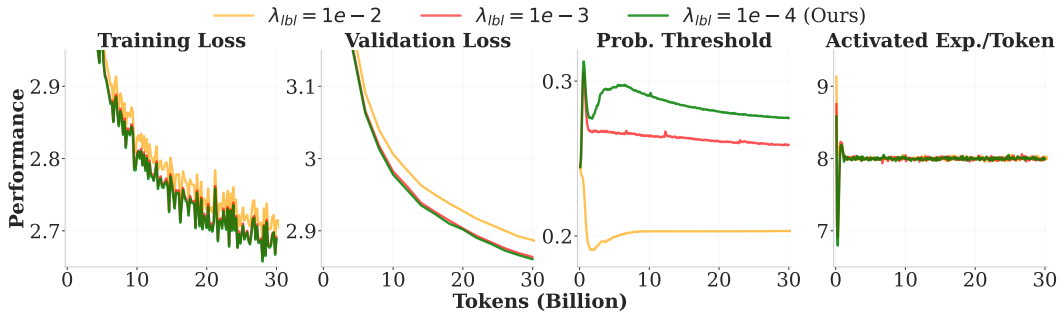


Figure 17: Load Balancing Loss coefficient tuning results. A small coefficient of 1×10^{-4} achieves the best performance.

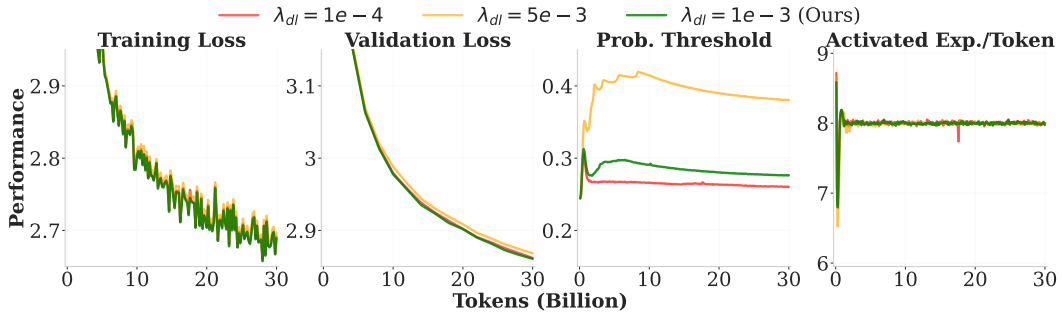


Figure 18: Dynamic Loss coefficient tuning results. A moderate coefficient of 1×10^{-3} achieves the best performance for DTop- p .

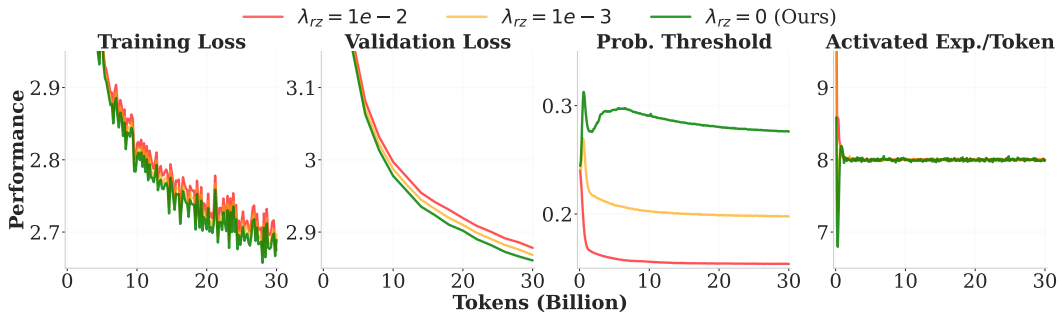


Figure 19: Router Z-Loss coefficient tuning results. DTop- p performs best without Router Z-Loss ($\lambda_{rz} = 0$).